Coupled Ocean–Acoustic Prediction of Transmission Loss in a Continental Shelfbreak Region: Predictive Skill, Uncertainty Quantification, and Dynamical Sensitivities

Pierre F. J. Lermusiaux, Jinshan Xu, Chi-Fang Chen, Sen Jan, Linus Y. Chiu, and Yiing-Jang Yang

***Abstract*—In this paper, we quantify the dynamical causes and uncertainties of striking differences in acoustic transmission data collected on the shelf and shelfbreak in the northeastern Taiwan region within the context of the 2008 Quantifying, Predicting, and Exploiting Uncertainty (QPE 2008) pilot experiment. To do so, we employ our coupled oceanographic (4-D) and acoustic (Nx2-D) modeling systems with ocean data assimilation and a best-fit depth-dependent geoacoustic model. Predictions are compared to the measured acoustic data, showing skill. Using an ensemble approach, we study the sensitivity of our results to uncertainties in several factors, including geoacoustic parameters, bottom layer thickness, bathymetry, and ocean conditions. We find that the lack of signal received on the shelfbreak is due to a 20-dB increase in transmission loss (TL) caused by bottom trapping of sound energy during up-slope transmissions over the complex and deeper bathymetry. Sensitivity studies on sediment properties show larger but isotropic TL variations on the shelf and smaller but more anisotropic TL variations over the shelfbreak. Sediment sound-speed uncertainties affect the shape of the probability density functions of the TLs more than uncertainties in sediment densities and attenuations. Diverse thicknesses of sediments lead to only limited effects on the TL. The small bathymetric data uncertainty is modeled and also leads to small TL variations. We discover that the initial transport conditions in the Taiwan Strait can affect acoustic transmissions downstream more than 100 km away, especially above the shelfbreak. Simulations also reveal internal tides and we quantify their spatial and temporal effects on the ocean and acoustic fields. One type of predicted waves are semidiurnal shelfbreak internal tides propagating up-slope with wavelengths around 40–80 km, horizontal phase speeds of 0.5–1 m/s, and vertical peak-to-peak displacements of isotherms of 20–60 m. These waves lead to variations of broadband TL estimates over 5–6-km range that are more isotropic and on bearing average larger (up to 5–8-dB amplitudes) on the shelf than on the complex shelfbreak where the TL varies rapidly with bearing angles.**

***Index Terms*—Coastal ocean, data assimilation, distributed and many-task computing, ensemble prediction, interdisciplinary modeling, internal tides, shelf and shelfbreak sound propagation, uncertainty quantification, underwater acoustics.**

Manuscript received January 14, 2010; revised August 04, 2010; accepted August 12, 2010. Date of current version November 30, 2010. This work was supported by the U.S. Office of Naval Research under the QPE Grants N00014-07-1-0241 and N00014-08-1-0586 to the Massachusetts Institute of Technology (MIT), Cambridge.

Associate Editor: J. F. Lynch.

P. F. J. Lermusiaux and J. Xu are with the Department of Mechanical Engineering, Massachusetts Institute of Technology, Cambridge, MA 02139 USA (e-mail: pierrel@mit.edu; jinshan@mit.edu).

C.-F. Chen, S. Jan, and L. Y. Chiu are with the National Taiwan University, Taipei 106, Taiwan.

Y.-J. Yang is with the Department of Marine Science, Chinese Naval Academy, Kaohsiung 813, Taiwan.

Color versions of one or more of the figures in this paper are available online at http://ieeexplore.ieee.org.

Digital Object Identifier 10.1109/JOE.2010.2068611

I. Introductionand Motivation

As one of the major application of underwater acoustics, sonar performance prediction requires modeling the acoustic field evolution. In the littoral environment, the time and space scales relevant for such predictions can be minutes to a week and hundreds of meters to tens of kilometers. The parameters include the 4-D ocean and seabed fields. They are difficult to predict and can have significant uncertainties [1], [2]. Methods and systems that forecast the ocean, the seabed, and the acoustics in an integrated fashion have only been developed and utilized recently [3]–[7]. Acoustic data were previously not available for evaluations of such systems. An objective of the present investigation is to compare predictions of such coupled systems to *in situ* acoustic data. Even though important, such comparisons had not been done before.

Our approach is based on coupling realistic data-assimilative environmental and acoustic propagation models with distributed, parallel ensemble simulations, as developed in [5], [6], [8], and [9]. The adjective "coupled" is here used in the sense of coupled partial differential equations (PDEs) or coupled system of PDEs, e.g., [10]–[12]. This approach was applied with adaptive sampling and onboard routing within the 2005 Focused Acoustic Forecasting (FAF05) exercise [13]. During the 2007 Persistent Littoral Undersea Surveillance Network (PN07) exercise in Dabob Bay, acoustic transmission loss (TL) fields were also coupled to data-assimilative ocean fields by Xu *et al.* [14] so as to characterize the impact of wind forcing and tidal forcing on acoustic fields and performance. Within the scope of the 2007 Battlespace Preparation (BP07), Lam *et al.* [15] coupled acoustic and ocean models at sea in real time, Rixen *et al.* [16] utilized super-ensemble prediction techniques for acoustic inversion and tomography, Carriére *et al.* [17] investigated full-field tomography and tracking, and Martins and Jesus [18] studied acoustic prediction as a Bayesian estimation problem. The New England Shelbfreak front region, e.g., [19]–[21], and the shallow Asian Seas, e.g., [22]–[26], have also seen major ocean and acoustic studies with coordinated sampling. The results of all these efforts show that ocean variability can considerably influence acoustic propagation properties both in time and in space. Acoustic propagation in

shallow water is also known to be strongly affected by multiple seabed interactions and bathymetry effects [27]. In continental shelfbreak regions, the seabed and bathymetry are complex and not well known. Uncertainties in geoacoustic modeling usually come from the imperfect knowledge of the true thicknesses and properties of the sediment and rock layers. Studying and quantifying the sensitivity of our coupled predictions to key ocean and geoacoustic uncertainties is another objective of our present effort.

Our investigations are parts of the Quantifying, Predicting, and Exploiting Uncertainty (QPE) initiative which aims to integrate probabilistic performance prediction, coupled ocean–acoustic modeling, multidisciplinary data assimilation, and autonomous ocean platforms to improve performance prediction and reduce detection uncertainties. Our focus is on the QPE 2008 pilot exercise [28] carried out on the continental shelf and slope of northeast Taiwan in September 2008. The main goals of this 2008 exercise were to test systems and methodologies to measure and forecast the baseline regional ocean variabilities and uncertainties, as well as their impact on low-frequency (100–1000 Hz) acoustic propagation conditions. Two main locations were chosen for the exercise: one on the continental shelf and the other on the shelfbreak. Interestingly, the TL over ranges of 5–6 km over circular areas in these two regions were observed to be very different. This occurred even though the two circular areas overlapped in space. For example, no signal was obtained when the source was over the deeper water on the shelfbreak, and the measured mean and variability of the TL differed greatly in the two regions. To explain and quantify these observed behaviors, both acoustic and environmental dynamical modeling are required.

In this study, we utilize coupled oceanographic (4-D) and acoustic (Nx2-D; i.e., a 3-D space approximated with N centric vertical 2-D slices) full-field simulations to explain and quantify the mean and dynamic variability of midfrequency sound TLs observed during the QPE 2008 pilot experiment northeast of Taiwan. To do so, such coupled and realistic model estimates are for the first time compared to the underwater acoustic observations available. We also investigate the sensitivity of the TL and of its probability density function (pdf) to uncertainties in geoacoustic parameters, bathymetry, sediment layer thicknesses, and initial transports in the Taiwan Strait as well as to background sound-speed variability involving tidal effects. Each ensemble computations are high resolution in range, bearing angles, and time, and are completed for multiple locations and ocean conditions. Distributed parallel computing is employed [29]–[31].

In what follows, we first outline the QPE 2008 pilot experiment and the corresponding observations and coupled modeling systems (Section II). In Section III, the TL data and their variability with respect to positions and bearing angles are compared with our coupled oceanographic–acoustic modeling predictions. The uncertainties in the TL estimates due to various factors are also modeled and quantified, and the sensitivity of these TL estimates to ocean variability is computed and studied. The summary and conclusions are in Section IV. In the Appendixes, we first outline the coupled model equations and their respective parameters (Appendix I) and then summarize numerical procedures for such coupled and realistic modeling, including intensive parallel computing (Appendix II).

II. Real-Time Experiment, *In Situ* Observations and Coupled Modeling Systems

The QPE 2008 pilot cruise was carried out on the continental shelf and slope of northeast Taiwan (Fig. 1). Most of the acoustic propagation experiments were conducted inside the rectangular boxed region just north of 25.5° N, 122.5° E. Our regional dynamics and modeling focus was the continental shelf and slope northeast of Taiwan, and especially the Cold Dome (e.g., [32]), its dynamics, variabilities and uncertainties, as well as an impact of this environment on low/midfrequency (100–1000 Hz) acoustic propagation. In the region, a large number of ocean processes can occur simultaneously, very energetically, and on multiple scales [28], [33]–[35]. The ocean observations, the coupled ocean–acoustic modeling systems used for real-time predictions, and the acoustic observations are described next.

A. Ocean Observations

The pilot experiment involved three separate cruises to collect ocean environmental data [see Fig. 1(a) for the conductivity–temperature–depth (CTD) station positions]. The solid dots are for the OR1 cruises: leg 1 was operated between the Ilan Ridge and the Main Study Area during September 2–4 while leg 2 was in the Main Study Area during September 6–11. The stars and circles indicate the stations that the vessels operated during August 22–27 (respectively, the OR2 northeast of Taiwan and the OR3 in the Taiwan Strait). As soon as available, these CTD measurements, as well as other measurements were assimilated in our simulations.

B. Real-Time Modeling Systems and Coupled Predictions

In real time, we completed sustained coupled-oceanographic (4-D) and acoustic (Nx2-D) full-field simulations for a seven-day-long period [33], each day selecting a subset of these simulations as the acoustic–ocean forecast for the next two days. Our simulations utilized the Massachusetts Institute of Technology (MIT) Multidisciplinary Simulation, Estimation, and Assimilation System (MSEAS, [31]). For the ocean dynamics, it employs a free-surface and two-way nested primitive-equation code [36] (a significant upgrade of the rigid-lid Harvard primitive-equation model [37], [38]); its equations are in Appendix I-A). The MSEAS system also involves a coastal objective analysis scheme based on fast-marching methods [39]; an optimal interpolation scheme and error subspace statistical estimation (ESSE) system [40]–[43] for data assimilation, optimization, and adaptive sampling; schemes for uncertainty predictions based on dynamically orthogonal equations [44]; multiple biological models [45]; and several acoustic models.

The QPE ocean simulations were forced with barotropic tidal flows [46] at open ocean boundaries, in the present setup with the semidiurnal constituent M2 only (the constituents S2, K1, O1, N2, and K2 were also used in the real-time simulations for the intensive observation period in 2009 [47]). The atmospheric forcing at the air–sea interface was a combination of the Coupled Ocean/Atmospheric Mesoscale Prediction System (COAMPS) (wind stress) and the Navy Operational

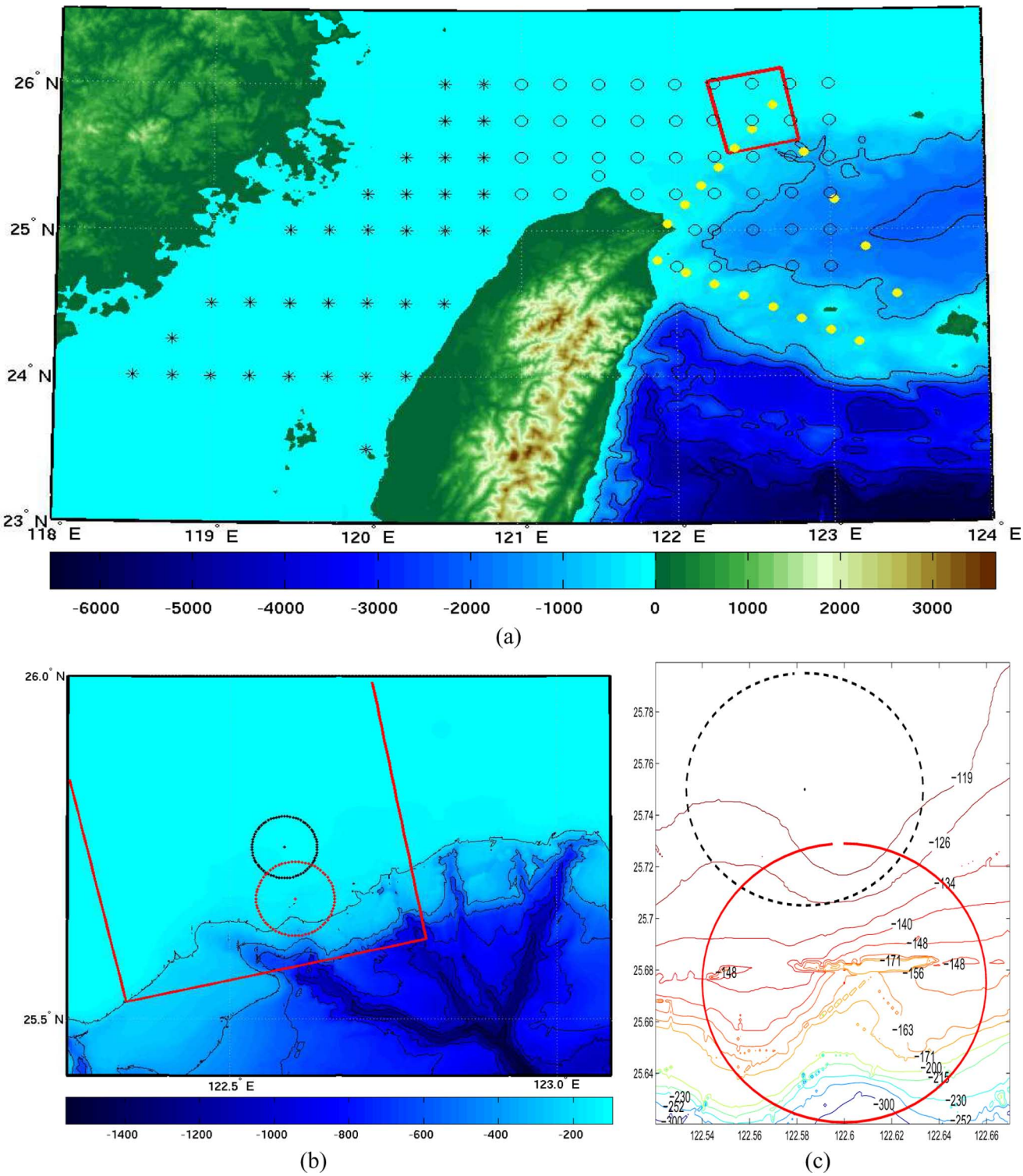

Fig. 1. (a) QPE pilot experiment—CTD stations and main study area. The intensive acoustic region is identified by the solid box. The solid dots are CTD stations for the OR1 Leg 1,2 cruises, stars for the OR2 cruise, and circles for the OR3 cruise. (b) Bathymetry (meters) of the Acoustic Experiment region overlaid with the two planned tracks of the OASIS Mobile Acoustic Source (OMAS) circle runs, referred to as events A and B. (c) Bathymetry (meters) at locations of events A and B.

Global Atmospheric Prediction System (NOGAPS) (heat-flux, E-P) forcing. Fields were initialized with the OR2 and OR3 CTD data merged with a summer climatology created using June–August profiles and the HydroBase2 software [48]. The bathymetry used was the National Center for Ocean Research (NCOR, Taiwan) bathymetry (S. Jan, personal communication) merged with interpolated high-resolution bathymetry data provided by the Center for Coastal and Ocean Mapping, University of New Hampshire, Durham [49]. The OR1 CTD and the Seasoar data were assimilated when available. During the preparation of the exercise, we found that the net transport between Taiwan and mainland China can have a significant

influence on the formation and strength of the cold dome, especially just north of Taiwan. To account for the corresponding uncertainty in real time, three different initial transport cases were utilized for each ocean forecast (of course, boundary conditions vary in time with a radiation condition [50], but the radiation condition is applied to the departure from this initial estimate [36], [51], which remains fixed). The skill of ocean predictions was computed in real time [52] and forecasts were found better than persistence. The values of the numerical and physical parameters are listed in Table III in Appendix I-A.

The ocean forecasts and their uncertainties were used as inputs to the acoustic simulations. For the acoustics, the bathymetry data used were that of the ocean model, but at the full resolution provided by the Center for Coastal and Ocean Mapping with up to 100-m resolution in the main study region [49]. Acoustic simulations were performed with the coupled SACLANTCEN (La Spezia, Italy) normal mode propagation loss model (C-SNAP) [53] using the sound-speed fields of MSEAS as parameters (see Appendixes I-B and II). In real time [33], TL forecasts were provided along five 20-km-long acoustic propagation paths which had been preselected to explore the variability in this region. As a whole, the QPE scientific team successfully resolved the Cold Dome, preformed data transfer in real time, and forecasted oceanographic and acoustic propagation conditions daily, including uncertainties in ocean fields due to uncertainty in the Taiwan Strait transport. Our acoustic–ocean modeling and its results are described in Section III.

C. Acoustic Propagation Observations

The acoustic propagation experiments were conducted during leg 2 of the pilot cruise on OR1. The Ocean Acoustical Services and Instrumentation Systems (OASIS) mobile acoustic sources (OMAS) disposable vehicles were utilized as sound sources [54]. The receivers included standard U.S. Navy sonobuoys and the National Taiwan University (NTU) vertical line array (VLA). Four OMAS events were carried out: two on the shelf along relatively constant headings and depths and two in circular tracks around the shelfbreak region.

The first two "constant-heading" events conducted on the shelf occurred at approximately 110–130-m depth. The OMAS moved at a speed of 5 kn. These data were used to tune our coupled systems at different ranges (see Section III). The other two acoustic events were the two circular OMAS runs: events A and B, as shown in Fig. 1(b). The northern and southern circles are the nominal event A and B tracks, respectively. The programmed radius of event A was set to 5 km and that of event B to 6 km. The OMAS vehicles and the sonobuoys were set to run at 61 m in depth. The northern circle was centered at approximately 110 m in depth, and covered a relatively flat, slightly sloping bottom. The southern circle was positioned over the steeply breaking shelf. Fig. 2(a) presents TL measurements collected from the two runs: the blue curve denotes the measured 1100-Hz TL as a function bearing angle with 15° bearing sector averages for event A; the red curve is the same, but for the 900-Hz TL data for event B. Note that the TL data here are in the units of dB re 1 m away from source level and are the peak of the matched-filter output. Small linear range corrections are applied to obtain the measured TL estimate at the range of 6 km. The TL of event A varies somewhat with the bearing angle, showing an increased TL in the northeastern direction. Interestingly, during event B (southern circle positioned over the shelfbreak), no signal was observed when the OMAS source was in the deeper waters. In addition, considering the arcs over the shelf only, the mean of the TL data was 2–5 dB larger for event B (shelfbreak run) than for the arc of event A (shelf run). Two of our goals are to model and quantify such observations, and to investigate the variation of the TL estimates due to uncertainties in the sediments, bathymetry, and ocean water-column variation.

III. Results

Our simulations start with the 4-D ocean sound-speed fields provided by the MIT MSEAS system for the period of September 1–12, 2008 (Section II-B). Acoustic TL fields were computed using C-SNAP in 120 bearing directions (with a three-degree resolution in azimuth, 10 m in range and 2 m in depth; see Appendix I-B) for both events A and B, at frequencies of 1100 and 900 Hz, respectively. We completed a number of Nx2-D computations with different center positions (not shown). The best fit for these centers of the two simulated OMAS circles was at 25° 39.8′ N, 122° 35.76′ E) and 25° 44.55′ N, 122° 33.90′ E), with radius of 6 km, respectively. These locations are in accord with the mean estimates of the positions of the slightly moving receivers' tracks [28]. The sources and receivers were set at 61-m depth below the sea surface to fit the sea configuration. TLs were computed at positions that were ± 600 m in range and ± 5 m around the depth of the receiver. The average predicted TL within these horizontal and depth ranges was then set to be our TL estimate because it is a good approximation [55] to the 10% bandwidth of frequency averaging that occurred in the real *in situ* broadband propagation. All of the Nx2-D TL estimates that we show in this paper are broadband estimates, but we often simply refer to them as TL.

We first tuned our model fields to TL observations for the two "constant-bearing, along-bathymetry" events, using a large set of simulations. These observations allowed tuning at different ranges and provided guidance for the geoacoustic model parameters. At the end, we obtained good fits at all measured ranges. With this fitted model, we can justify comparing model results to measurements along circular OMAS runs, i.e., observations at relatively fixed ranges but with propagation angles diversity.

Ensembles of coupled ocean–acoustic simulations were also completed for the two circular OMAS runs. The best results are illustrated in Fig. 2(b), with event A at 12:00:00Z, September 8, 2008, and event B at 15:00:00Z, September 8, 2008. Shown are our broadband TL estimates for the time and location of the two events, for all bearing angles. All (geo)acoustic parameters used in this simulation are given in Appendix I-B. If we consider only the range of bearing angles for which a signal was received at sea from the OMAS runs, our mean TL estimates for events A and B are about 77–81 and 79–85 dB, respectively. These predicted means are in good agreement with the mean data received [Fig. 2(a)]. The two are within 1–3 dB, which is within the uncertainties of our coupled acoustic–ocean

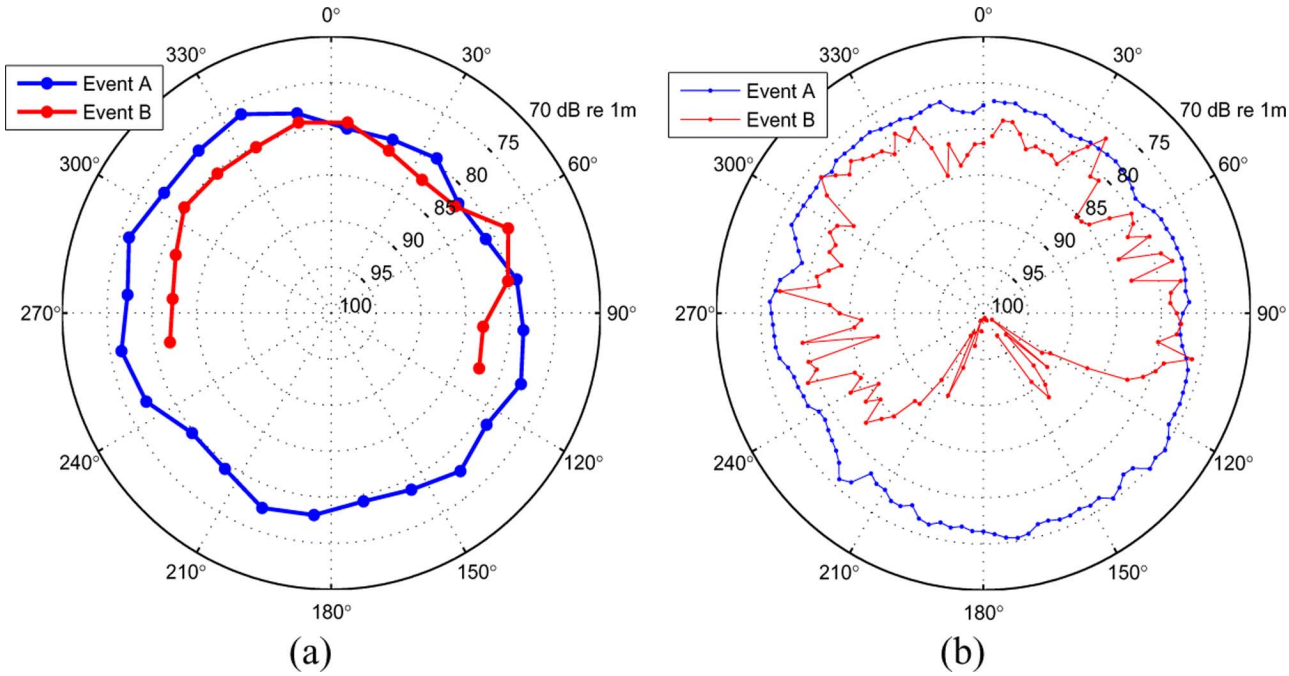

Fig. 2. (a) Measured mean TL of event A (blue, with observed bearing-averaged $\sigma = 1.8$ dB) and event B (red, with $\sigma = 2.4$ dB) (Abbot and Emerson, personal communication). (b) Coupled ocean (4-D) and acoustics (Nx2-D) simulations of the mean TL of event A (blue, with bearing averaged $\sigma = 1.23$ dB) at 12:00:00Z, September 8, 2008, and event B (red, with $\sigma = 2.33$ dB in the bearing angle ranges: $\geq 260°$ or $\leq 110°$; $\sigma = 7.87$ dB for whole circle) at 15:00:00Z, September 8, 2008. The main central ocean and acoustic parameters used in these simulations are given in Appendix I.

simulations (Section III). In addition to the mean values, spatial patterns are also captured. For example, for event A, one notes the increased TL in the northeastern direction (225° to 45°), in accord with the data [Fig. 2(a)]: this is linked to ocean variability as shown in Section III-D. For event B, our simulated mean TL on the shelf is also lower by 2–5 dB than that of event A along the same angles, as was observed: this result is linked to seabed properties (Section III-A). The statistics of the measurements and model estimates are not compared in further details, because in the measurements, the statistics involves the dominant arrivals with inherently few degrees of freedom but includes also the variations in depth and position of the source and the receiver which add degrees of freedom, while in the modeling, it involves the 200-Hz broadband averages with various rays interacting with the bottom and so inherently more degrees of freedom but fixed source and receiver.

The bathymetry data [see Fig. 1(c)] along bearing angles of 120°–230° shows depth variations from 150 m to more than 300 m. In our coupled modeling results, this leads to a mean TL estimate for event B that is higher by 15–20 dB than the mean TL of event A along the same angles [Fig. 2(b)]. We expect that this explains why there was no reception during the event B run when the OMAS went over this deeper shelfbreak region. At these angles, this leads to an up-slope transmission which causes extensive TL. This is a first-order effect [56], which also occurred when we used a climatological ocean (even though the climatological TL differs by 1–5 dB from the time-mean-ocean TL). Since the water-column, seabed, and bathymetric features are uncertain, we study and quantify next the sensitivity of our broadband TL estimates to uncertainties in geoacoustic parameters (sediment thickness and sediment types), bathymetry, and uncertainty and variability of the ocean sound-speed fields (Taiwan Strait transport and tidal dynamics). For each uncertainty factor, we compute the standard deviations of our TL estimates (assuming all other factors constant and perfectly known). Of course, these standard deviations differ from the standard deviations of the TL measured at sea. This is because the standard deviations of the measured TL correspond only to variations in the ocean and in the positions/bearing during the given OMAS circle run (assuming the bathy and seabed properties are fixed during that time).

A. TL Sensitivities to Uncertainties in the Geoacoustic Model—Sediment Types and Thicknesses

Uncertain factors in the geoacoustic model that lead to uncertainties in the TL estimates include the thicknesses and properties of the sediment and rock layers. At higher sound frequencies, the first few to tens of meters of sediments matter most. At lower frequencies, the whole sediment column and underlying rocks often matter. A challenge for precise modeling of sound propagation in this region is the lack of knowledge of the geoacoustic parameters. For our frequencies (900 and 1110 Hz), we evaluated and compared more than 30 sediment models. Here we only report a few of them including sand, muddy-sand, silty-clay, and hybrid models in Tables I and II. Specifically, Table I gives three sediment types and a half-space basement, while Table II gives our best fit so far, a hybrid and depth-dependent model. For each sediment, note that the first line corresponds to the optimum values we obtained using the hybrid model, while the second line indicates the deviation ranges of the parameter values that we tested on. The first three sediments followed Hamilton's models [57], [58]. The hybrid depth-dependent models were the best fit results of our multiple comparisons to data aiming to optimize parameters (three

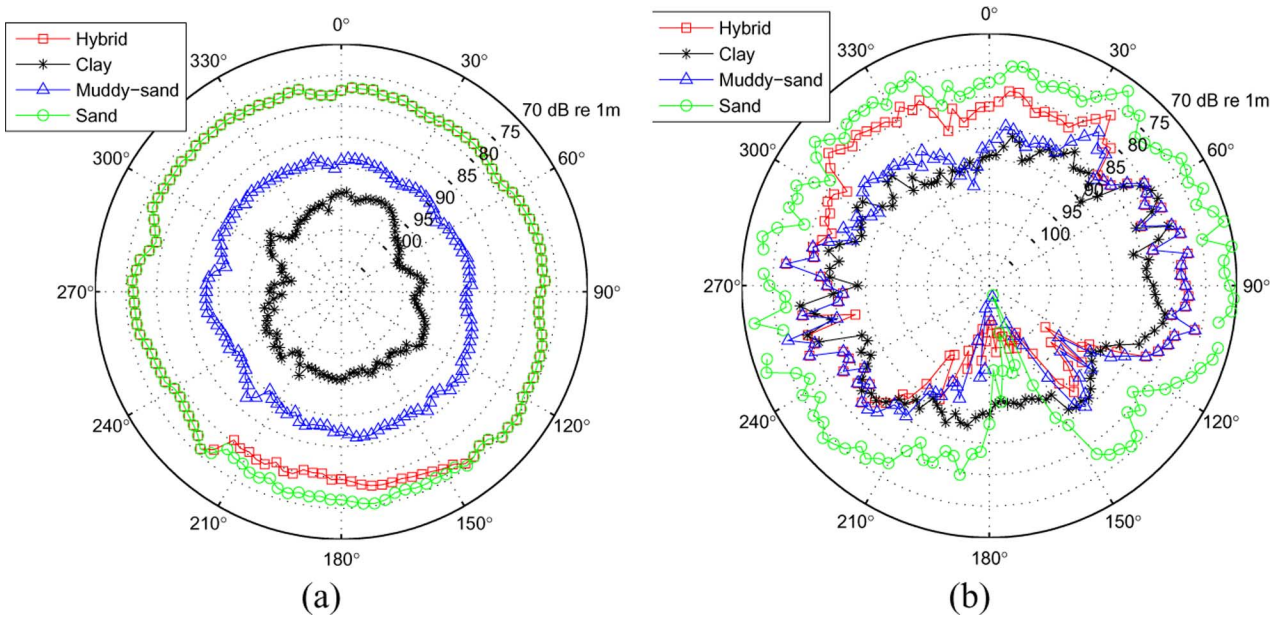

Fig. 3. Nx2-D TL simulations of events A and B, illustrating effects of different sediments models (and keeping all other factors constant: in particular, the sediment thickness is set to 20 m). The four different sediments discussed here were: depth-dependent (hybrid) model with variable sediments, sand, muddy sand, and silty clay. With these sediment variations, one obtains a standard deviation for event A of $\sigma_{\mathrm{TL}_{\mathrm{sediment}}}(\theta) = 9.55$ dB and for event B of $\sigma_{\mathrm{TL}_{\mathrm{sediment}}}(\theta) = 5.81$ dB. The central ocean fields are at 12:00:00Z, September 8, 2008. Note that $\sigma_{\mathrm{TL}_{x\ \mathrm{variable}}}(\theta)$ denotes the bearing average over θ of the standard deviation of the TL over the x-variable. The same notation is used in all subsequent captions.

TABLE I
SEABED PROPERTIES OF THREE DIFFERENT SEDIMENT MODELS AND OF THE BASEMENT. FOR EACH SEDIMENT MODEL: THE FIRST LINE GIVES THE OPTIMUM VALUES WE OBTAINED, THE SECOND LINE INDICATES THE DEVIATION RANGES OF THE PARAMETER VALUES THAT WE TESTED ON. OVERALL, MORE THAN 30 SEDIMENT MODEL VALUES WERE COMPARED

	Cp (m/s)	ρ (×10³ kg/m³)	Attn (dB/λ)
Sand	1562	1.9	0.90
	1550~1650		0.25~ 1.0
Muddy-Sand	1549	1.488	1.15
	1540~1575		0.4 ~1.25
Clay	1460	1.421	0.1
			0.03 ~ 0.2
Basement	1800	2.0	0.5

TABLE II
DEPTH-DEPENDENT SEDIMENT MODEL, RESULTING OF A BEST FIT OF OUR COUPLED OCEAN–ACOUSTIC MODELS TO TL OBSERVATIONS. NOTE THAT MORE THAN TEN SETS OF TWO TRANSITION DEPTHS WERE TESTED. ONLY THE BEST FIT IS REPORTED HERE

Shallow water	Z < 140 m	Sand
Shelf Break	140 < Z < 210 m	Muddy-sand
Continental Slope	Z > 210 m	Clay

sediment types and two transition depths) and of interactions with Heaney, Holland, and Chen (personal communications). A similar hybrid model was also obtained by Heaney [59].

In Fig. 3, we illustrate how sediment layers affect our TL estimates for both events A and B, showing the results for four of the models we evaluated (see Tables I and II). The sediment thickness is set to 20 m in all cases. We find that the four models have different impact on the shelf and shelfbreak.

For event A on the shelf, the four sediments lead to distributions of TL variation with bearing angles that are very similar. The sediment types shown lead to overall isotropic TL differences of 5–15 dB in all directions. The average standard deviation is 9.55 dB.

For event B on the shelfbreak, the average standard deviation is smaller, 5.81 dB, than for event A. The shapes of the four TL estimates are still similar, but a bit less than for event A. The TL deviations due to different sediments are estimated to be lesser along the shelfbreak (e.g., 5 dB or less) but a bit larger towards the shelf (e.g., about 7–8 dB along 330°) and for bearing angles of 120°–240°, which is over the deeper bathymetry region. In fact, the steepest bathymetries lead to a very localized amplification of TL uncertainties due to sediment uncertainties: TL deviations are maximum (30 dB) along the bearing angle of 180°. Nonetheless, all TL fields of event B for bearing angles of 120°–240° clearly show a much higher TL than in event A (on average, by about 20 dB), as was measured at sea [see Fig. 2(a)]. This implies that the sediment properties cannot alone explain the observed higher loss; they lead to secondary effects when compared to the bathymetry.

We also investigated the effects that uncertainties in the thicknesses of sediment layers have on our TL estimates. The results (plots not shown here) indicate that variations of 5–25 m in the sediment thicknesses have some limited effects only on the up-slope transmissions for the circle runs of both event A (less than 2-dB uncertainty) and event B (less than 2–3-dB uncertainty, except in the deeper region where it reaches 3–6 dB).

A first result of these sensitivity studies to uncertainties in sediment types and thicknesses is that neither of them can alone explain the lack of transmission for event B when the OMAS

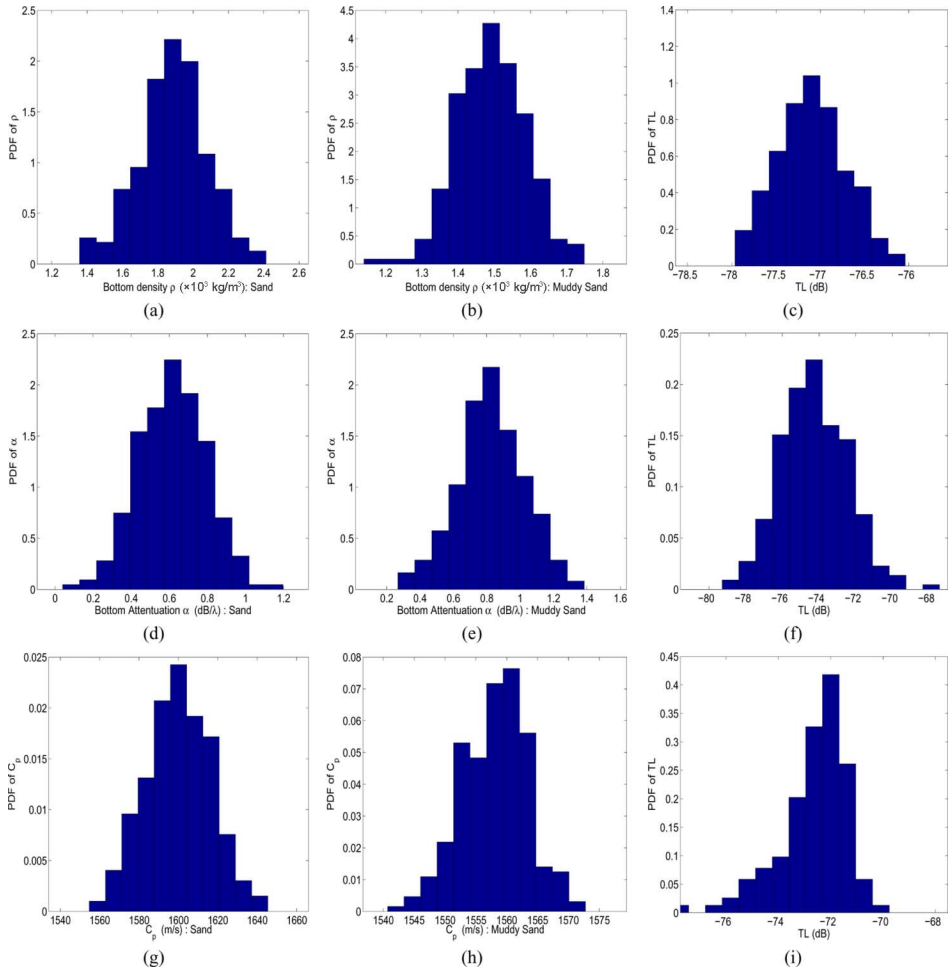

Fig. 4. TL uncertainties due to geoacoustics uncertainties, in accord with Tables I and II: (a) pdf of Gaussian realizations of bottom sediment density for sand; (b) pdf of Gaussian realizations of bottom sediment density for muddy sand; (c) pdf of TL corresponding to (a) and (b); (d) pdf of Gaussian realizations of bottom attenuation for sand; (e) pdf of Gaussian realizations of bottom attenuation for muddy sand; (f) pdf of TL corresponding to (d) and (e); (g) pdf of Gaussian realizations of bottom sound speed for sand; (h) pdf of Gaussian realizations of bottom sound speed for muddy sand; (i) pdf of TL corresponding to (g) and (h). The central ocean fields are at 12:00:00Z, September 8, 2008.

source moved over the deeper shelfbreak. A combination of both uncertainties (not shown) still does not change this conclusion. Therefore, the bathymetry itself is indeed responsible for the lack of transmission. A second result is that although the full geoacoustic inversion has not yet been completed for this site, our simple optimized hybrid sediment model and sediment thickness (20 m) with our 4-D simulations of the ocean sound speed lead to predicted estimates of the broadband TL that are in good agreement with the measurements [see Fig. 2(b)].

We completed a range of studies on TL uncertainties due to geoacoustics uncertainties, using Gaussian sediment sound speeds, densities, and attenuations that were in accord with the deviation ranges of Table I and the hybrid model of Table II. In all cases, we confirmed that uncertainties in sediment sound speeds have larger effects on TL uncertainties than uncertainties in sediment densities and attenuations, as expected in shallow water [58]. This is because sediment sound speeds strongly affect the critical angle and intromission angle of sound propagating in horizontally stratified layers. Examples are illustrated in Fig. 4: in each case, a total of 240 random realizations is used, for a shelf transmission over a 6-km distance, along bearing 0° relative to due north. Our normally distributed uncertainties in sediment densities (mean $= 1900$ kg/m^3, std $= 200$ kg/m^3 for sand; mean $= 1488$ kg/m^3, std $= 100$ kg/m^3 for muddy sand) lead to very small and overall Gaussian pdfs in TLs (mean $= -77.09$ dB, std $= 0.38$ dB), as shown in Fig. 4(a)–(c). Our normally distributed uncertainties in sediment attenuations are relatively larger (mean $= 0.62$ dB/λ, std $= 0.18$ dB/λ for sand; mean $= 0.82$ dB/λ, std $= 0.21$ dB/λ for muddy sand) and they lead to larger but still relatively Gaussian pdfs in TLs (mean $= -74.27$ dB, std $= 1.82$ dB); see Fig. 4(d)–(f).

Then, in Fig. 4(i), we show the pdf of TLs in response to our uncertainties in sediment sound speeds, again assuming Gaussian inputs for sand [mean $= 1600$ m/s and std $= 25$ m/s; Fig. 4(g)] and muddy sand [mean $= 1558$ m/s and std $= 9$ m/s; Fig. 4(h)]. The pdf of the TLs is then found to be skewed toward to higher losses (with mean $= -72.59$ dB, std $= 1.32$ dB). This can only be due to nonlinear interactions between the seabed sound-speed uncertainties and the 2-D acoustic field responses (pressure, phase). Such nonlinear effects can include effects of slower bottom sound speeds and of changes in angles of reflections off the seabed. Finally, we note that if we increased the standard deviations of the uncertainty in sediment sound speeds, the number of realizations of sediment sound speeds

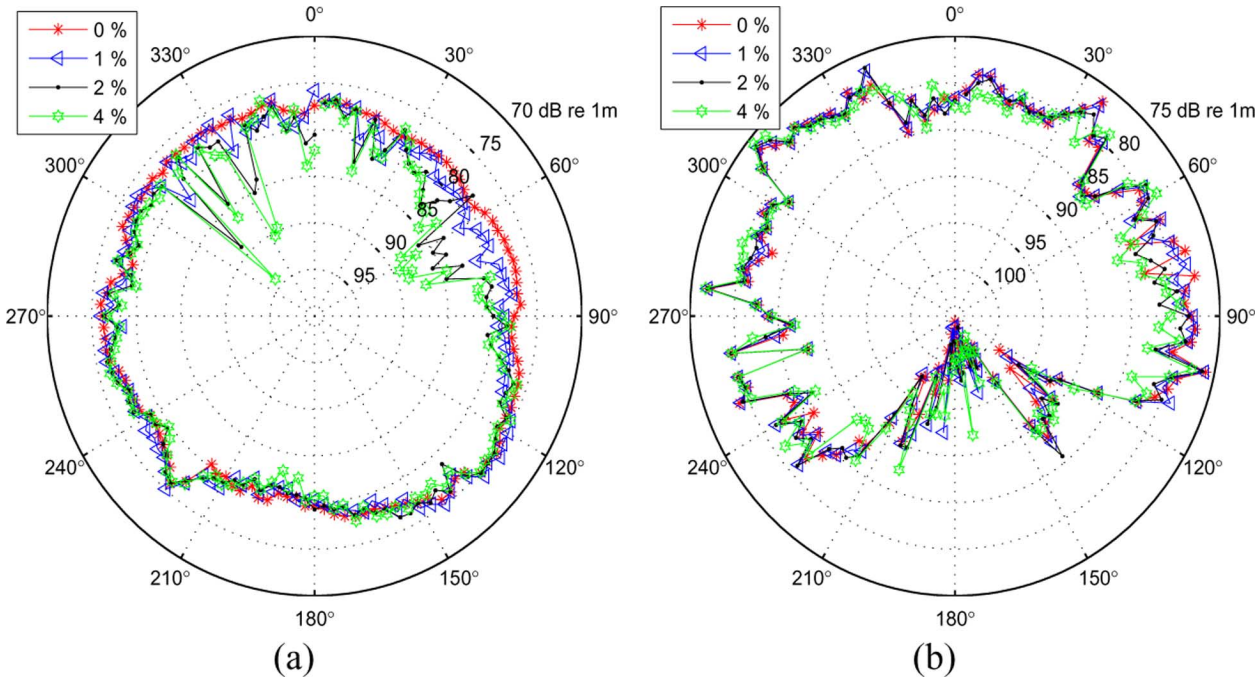

Fig. 5. Nx2-D TL simulations of event A ($\overline{\sigma_{\mathrm{TL}_{\mathrm{bathymetry}}}(\theta)} = 1.25$ dB) and event B ($\overline{\sigma_{\mathrm{TL}_{\mathrm{bathymetry}}}(\theta)} = 1.02$ dB) with different percentages of random perturbation on the 100-m resolution bathymetry data. The normally distributed random noise was added on the bathymetry with a variance proportional to the slope and to the local depth. The central ocean fields are at 12:00:00Z, September 8, 2008.

smaller than water-column sound speeds logically increased. We then found (figure not shown) that this led to a fully bimodal pdf of the TL on the shelf (one mode corresponding to the sediment sound speeds smaller than the water column sound speeds).

B. TL Sensitivities to Uncertainties in Bathymetry

We showed that the bathymetry is a first-order cause of the loss of acoustic reception in event B over the shelfbreak. Now, we estimate the TL variations due to uncertainties in this bathymetry. By comparing bathymetries of different resolutions and different origins, we obtained a general characteristic: errors in bathymetry are a function of the depth and slope. Therefore, we derived a simple model of the probability density of the bathymetry around its best measured estimate $D(x,y)$ (100-m resolution, [49]). This model consists of a zero mean Gaussian noise with standard deviation σ, a function of both the local slope and local depth, i.e.,

$$D(x,y;\omega) = D(x,y)[1+\epsilon\hat{S}\omega] = D(x,y)+\sigma(x,y)\omega \quad (1)$$

where $D(x,y;\omega)$ is a stochastic process, x and y are horizontal locations, Ω is the sample space containing the set of elementary random events $\omega \in \Omega \sim N(0,1)$, and

$$\sigma(x,y) = D(x,y)\epsilon\hat{S}(x,y) \quad (2)$$

$$\hat{S}(x,y) = \frac{|\nabla D(x,y)|}{\max(|\nabla D(x,y)|)} \quad (3)$$

where the latter is the normalized slope $\hat{S}(x,y) \subseteq [0\ 1]$ and ϵ is global parameter, representing the relative deviations. The simulation results with different realizations of this bathymetric uncertainty model are shown in Fig. 5, with ϵ chosen as 0%, 1%, 2%, and 4%. Each TL circular curve corresponds to a bathymetric noise with different percentages ϵ.

As a whole, for these levels of bathymetric uncertainties, we find that the uncertainties of our TL estimates are proportional to uncertainties in the bathymetry. Another result is that the general shape of the TL circular curves with bearing angles remains as obtained before. Bathymetric uncertainties do not alter the mean TL structure over the deeper ocean region.

C. TL Sensitivities to Uncertainties in the Ocean Water Column

In the following, we analyze effects of uncertainties in the mean water column on our acoustic TL predictions. We focus on uncertainties in the transport through the Taiwan Strait (ocean between mainland China and Taiwan, e.g., [60]). Even though the operational acoustic area is more than 100 km away northeast of the Taiwan Straits centerline, we had discovered (see Section II-B) that the strength of this Strait transport could have a significant influence on the Cold Dome region, especially just north of Taiwan [33]. If the initial Taiwan Strait transport was northward and of the order of 1 Sv or more, our simulations showed that the Kuroshio had limited intrusion over the shelfbreak northeast of Taiwan and the Cold Dome did not really form. However, if the initial Taiwan Strait transport was weaker or southward, we found that deeper and cooler Kuroshio waters upwelled on the shelf and the Cold Dome could form, the strength of this formation being a function of the transport. For the acoustics in the operational area northeast of Taiwan (see

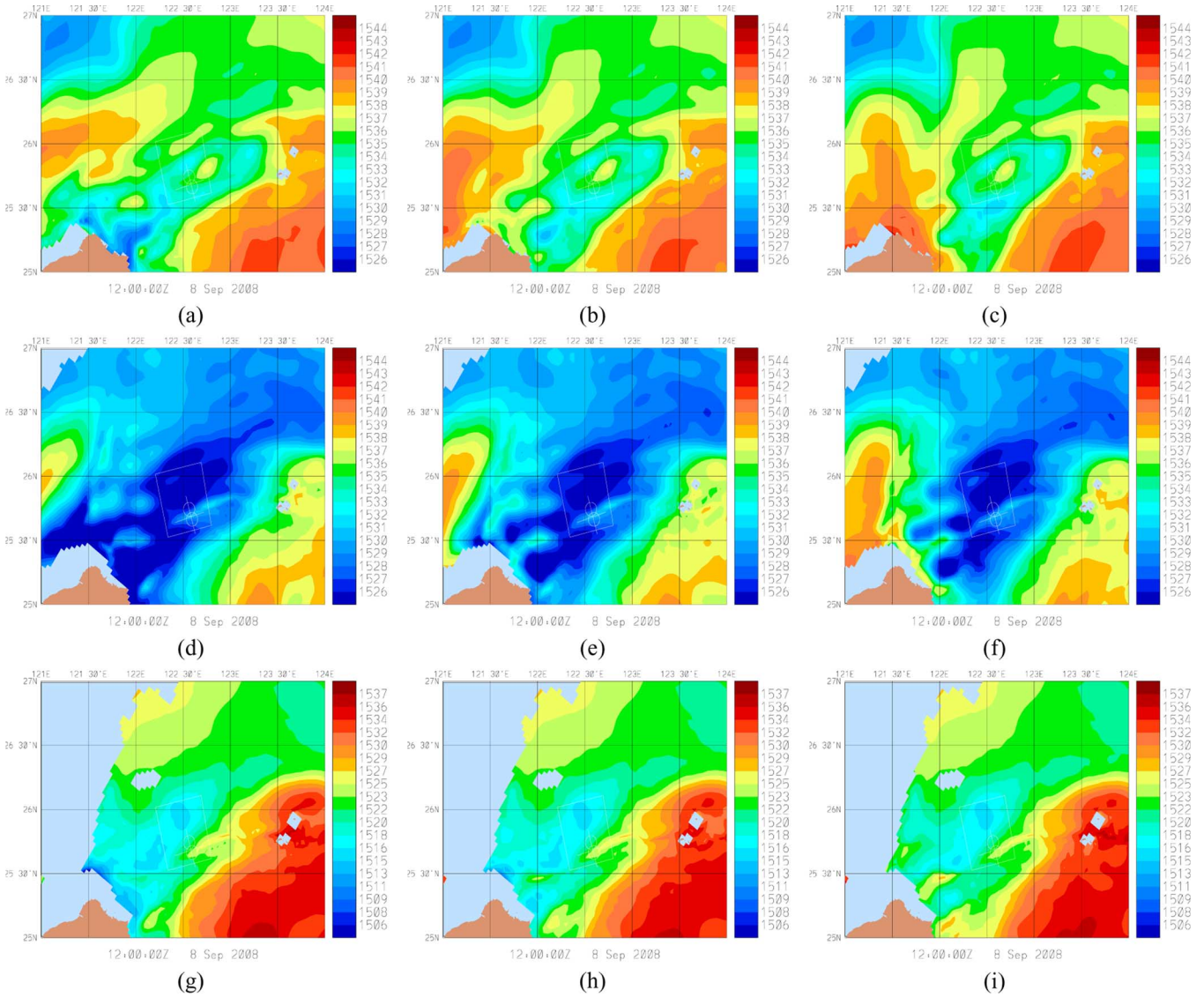

Fig. 6. Predicted ocean sound-speed field (colorbars in meters per second) at (a)–(c) 30-m, (d)–(f) 60-m, and (g)–(i) 90-m depth at 12:00:00Z, September 8, 2008, which is the day when events A and B occurred at sea. Each column corresponds to a different initial condition for the vertically averaged transport in the Taiwan Strait: first column—1 Sv S; second column—0 Sv; third column—1 Sv N.

Fig. 1), these different ocean forcing change the mean sound-speed field. They can thus have a significant impact on the TL estimates.

In real time, we considered three different initial transport conditions through the Taiwan Strait: an initial transport of 1 Sv northward, 1 Sv southward, and 0 Sv. Fig. 6 shows sound-speed fields in the QPE pilot experiment region at 30-, 60-, and 90-m depth (rows 1, 2, and 3 in Fig. 6, respectively) with different initial transport conditions through the Taiwan Strait (columns 1, 2, and 3 in Fig. 6, respectively). The main acoustic research area is denoted by a white rectangle frame. The three sound-speed fields appear more different at the depths of 30 and 60 m than at 90 m in part because the horizontal variability of sound speeds is larger at 90 m. The prediction skill for each of these initial conditions was computed in real time daily, based on comparisons with the available *in situ* data and sea surface temperature (SST) [52] for that day. On September 8, 2008, the 1 Sv south initial transport condition was chosen as the best ocean forecast.

Fig. 8 illustrates our Nx2-D acoustic simulations for events A and B, using the three different sound-speed backgrounds illustrated by the columns of Fig. 6. The geoacoustic model in all cases was the hybrid depth-dependent model with a 20-m thickness of sediment layer (see Section III-A). We find that the transport uncertainties cause different effects on the acoustic transmissions of events A and B (both occurred on September 8, 2008, at sea). The uncertainty in the ocean state due to the uncertainty in the initial conditions of the Taiwan Strait transport has more impact on our broadband TL estimates for the shelfbreak event B than for the shelf event A. For event A, our estimated TL variations along the different bearing angles reached about 1–3 dB, with a bearing-averaged standard deviation of 0.58 dB. However, for event B, our TL estimates varied almost evenly in all directions up to about 2–5 dB, with a bearing-averaged standard deviation of 1.21 dB.

In conclusion, these results first indicate that uncertainties in the Taiwan Strait transport lead to broadband TL uncertain-

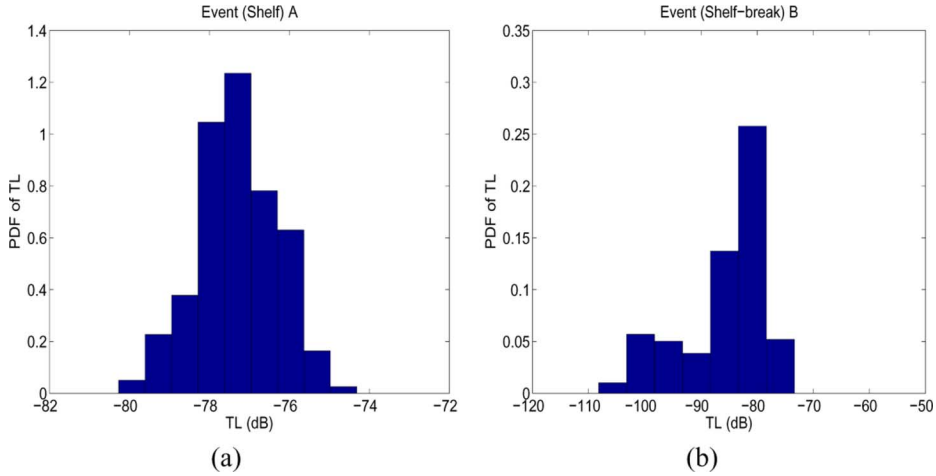

Fig. 7. TL uncertainties due to uncertainties of both sound propagation bearing angles and ocean initial conditions: (a) joint pdf of the TL for the shelf event A; (b) as (a) but for the shelfbreak event B. The central ocean fields are at 12:00:00Z, September 8, 2008.

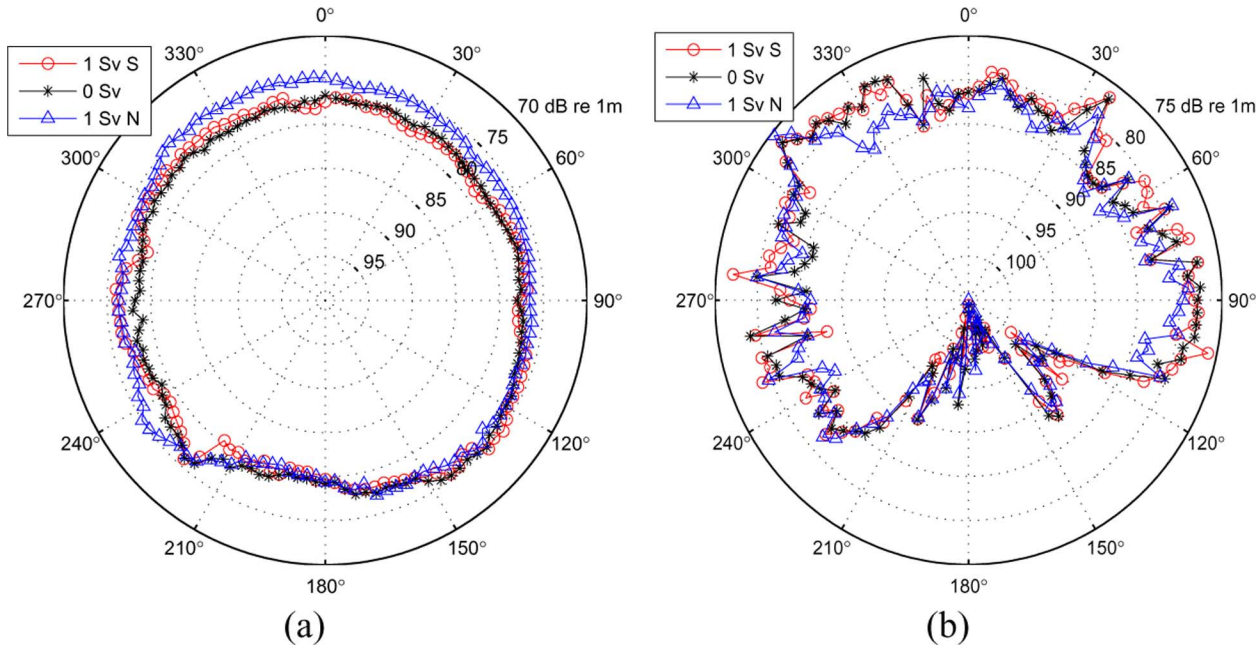

Fig. 8. Nx2-D TL simulations of event A ($\overline{\sigma_{\mathrm{TL}_{\mathrm{initial}}}(\theta)} = 0.58$ dB) and event B ($\overline{\sigma_{\mathrm{TL}_{\mathrm{initial}}}(\theta)} = 1.21$ dB) at 12:00:00Z, September 8, 2008, corresponding to different ocean field predictions (transport conditions between Taiwan and mainland China initialized at ± 1 or 0 Sv, as illustrated in Fig. 6) used as inputs for the background sound-speed field.

ties that are smaller on the shelf than on the shelfbreak. This is because the shelfbreak ocean dynamics is more sensitive to this transport than the shelf dynamics. Another result is that the shape of our broadband TL curve as a function of bearing angle does not vary much with these different ocean forecasts: it is mainly the mean TL which is affected. For each ocean transport, we still predict no signal received for event B when the OMAS passed over the deeper shelfbreak region.

If the acoustic modeling considered only a few bearing angles or if the given TL estimate was a range of the day with no bearing dependence, the TL variability with bearing angles would become uncertainty. We can estimate this pdf from our computations along 120 bearings. If we combine this bearing angle uncertainty with the uncertainty due to the transport in the Taiwan Strait, we obtain the pdfs shown in Fig. 7 for both the shelf and shelfbreak events. On the shelf [Fig. 7(a)], the joint pdf is relatively Gaussian, but slightly skewed towards lower loss. The joint mean TL is 77.3 dB and its joint standard deviation is 1 dB. On the shelfbreak [Fig. 7(b)], the joint pdf is bimodal, clearly showing the 20-dB difference in the two modes (the shelf versus slope directions). The joint mean TL is then 86.8 dB and its standard deviation is 7.5 dB.

D. TL Sensitivities to Tidal Dynamics in the Ocean Water Column

We now examine the variations of the TL field due to variability in the ocean, specifically tidal effects. We focus on internal tidal variability because our data-assimilative simulations revealed that semidiurnal frequencies in the ocean interior led to significant variations in the sound energy transmitted. First, we characterize this ocean variability, then we study its impact on the broadband sound transmission.

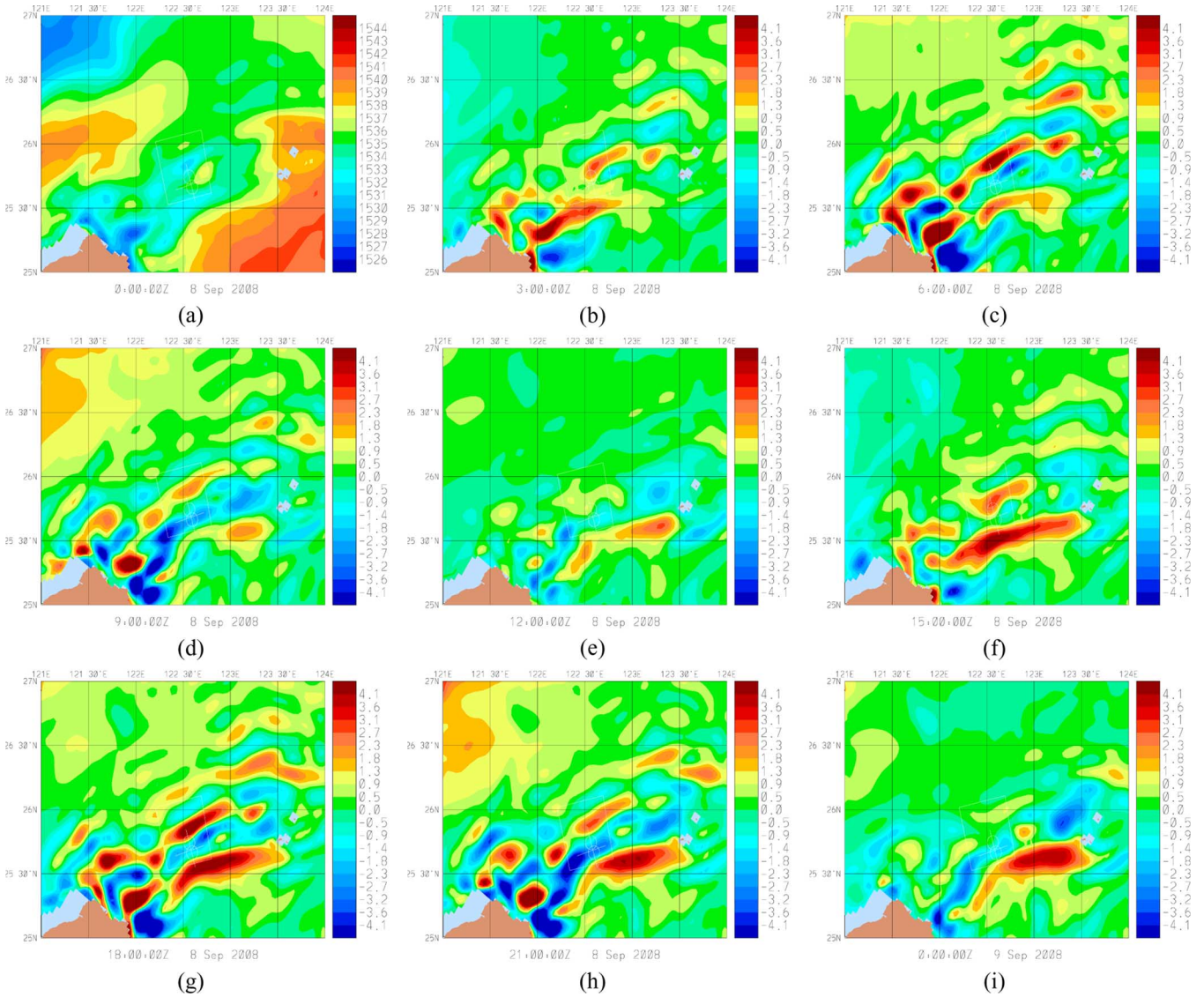

Fig. 9. Predicted sound-speed variability maps (colorbars in meters per second) from the central ocean fields at a depth of 30 m: (a)–(i) correspond to the times from 00:00:00Z September 8, 2008 to 00:00:00Z September 9, 2008 with 3-h intervals. (a) Total sound speed on 00:00:00Z September 8, 2008. (b)–(i) Differences between the subsequent 3-h sound-speed fields and this 00:00:00Z September 8, 2008 field.

Our simulations of the sound-speed field in the region over a 24-h period are illustrated in Fig. 9, on the day during which the acoustic events were measured at sea. Shown is the sound-speed variability at 30-m depth (in the upper layers of the main thermocline), every 3 h from 00:00:00Z September 8, 2008 to 00:00:00Z September 9, 2008. Fig. 9(a) is the total sound-speed map on 00:00:00Z September 8, 2008 while Fig. 9(b)-(i) are the differences between the subsequent 3-h maps and this 00:00:00Z September 8, 2008 map. Panels are ordered according to time such that: those on the main diagonal [Fig. 9(a), (e), and (i)] are 12 h apart from each other (close to being in phase for the semidiurnal tidal period); those on the first off-diagonals [Fig. 9(b), (f), (d), and (h)] are 3 h off from those on the main diagonal; and, those on the second off-diagonals [Fig. 9(c) and (g)] are 6-h off from those on the main diagonal (close to being in opposition of phase for the semidiurnal period).

The predicted sound-speed variability maps show the presence of internal tides oriented along the shelfbreak over more than a 200-km extent. They propagate up-slope and our simulations predict that their wavelength is around 40–80 km and semidiurnal phase speeds of 0.5 to about 1 m/s in the horizontal direction, which agree with previous estimates in the region, e.g., [24] and [35]. These maps also indicate that the shelfbreak internal tide patterns affecting our acoustic region (the white rectangle) are weaker and not aligned with the tide patterns around the tip of Taiwan. Other internal patterns are also present in the Taiwan Strait. At other depths (e.g., 60 and 90 m, not shown), variations in time reveal similar properties. Overall, we find that the amplitude of shelfbreak internal tides decays as the waves propagate up the shelf but remain significant up to about the 80-m isobath. After 24 h [Fig. 9(i)], predicted variations also show effects of mesoscale features (eddies, fronts, etc.).

Figs. 10 and 11 illustrate the sound-speed variability in vertical sections along and across the shelfbreak direction, respectively. The locations of the two sections and the acoustic circles of events A and B are plotted inside the white rectangular box

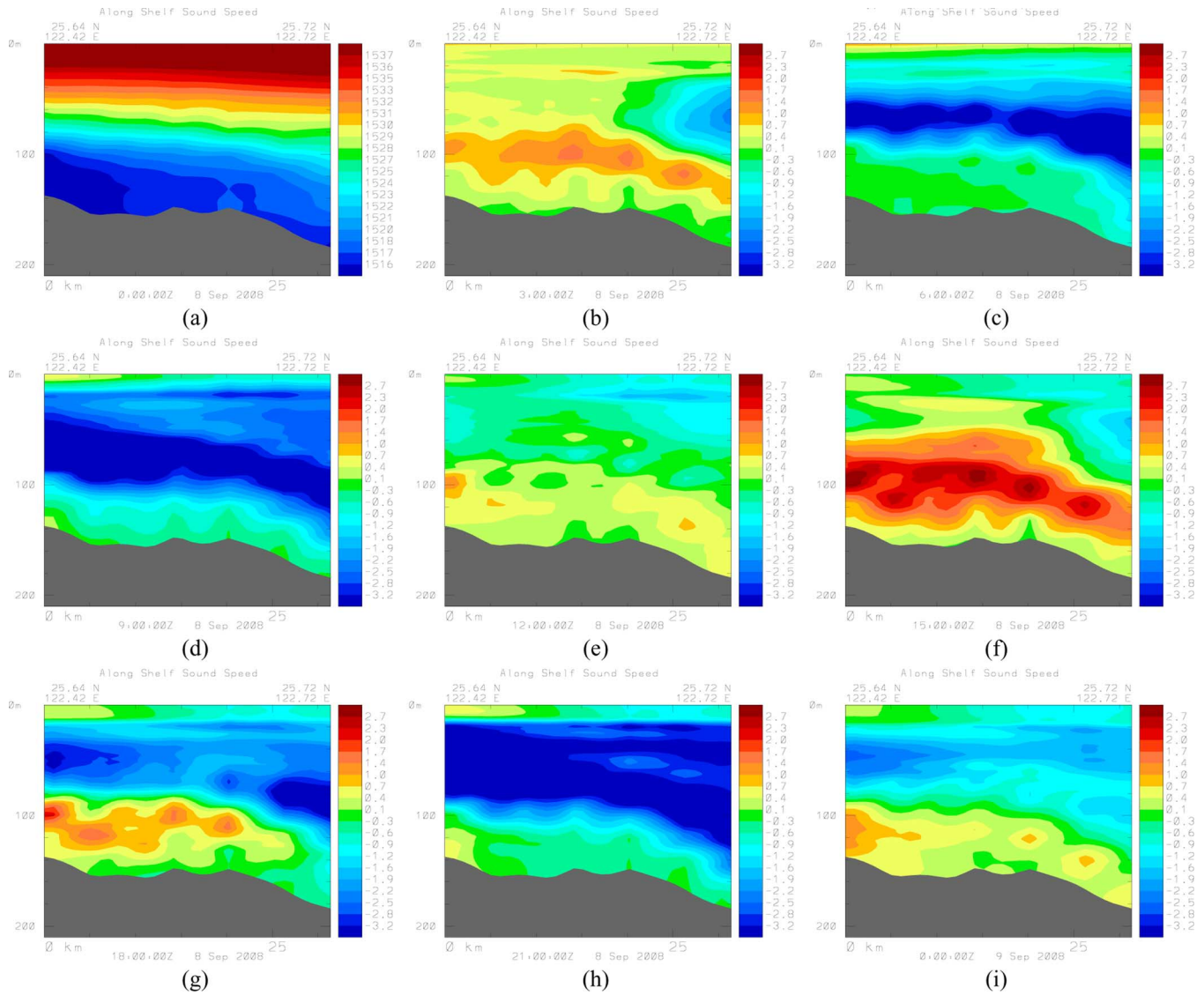

Fig. 10. Predicted sound-speed variability section from the central ocean fields, along the shelf, within the acoustic region (colorbars in meters per second): (a)–(i) times from 00:00:00Z September 8, 2008 to 00:00:00Z September 9, 2008 with 3-h intervals. (a) Total sound speed on 00:00:00Z September 8, 2008. (b)–(i) Differences between the subsequent fields and this 00:00:00Z September 8, 2008 field.

drawn on the maps of Figs. 6 and 9. Panels in Figs. 10 and 11 are still shown every 3 h on September 8, 2008: panel (a) is the total sound-speed section on 00:00:00Z September 8, 2008, while the other eight panels (b)–(i) are the differences between the subsequent 3-h sound speeds and this 00:00:00Z September 8, 2008 sound speed.

Within the section along the shelfbreak (Fig. 10), one detects the crest and trough of wave patterns: they are aligned with the section and concentrated around the main thermocline. As shown by the 3-h difference fields [Fig. 10(b)–(i)], the patterns are clearly depth dependent (baroclinic) and of tidal period (e.g., see the negative and positive anomalies on the upper and lower first diagonals of Fig. 10, respectively). This confirms the internal tide pattern. This signal is not small, and the largest sound-speed amplitudes are around 4 m/s (peak-to-peak around 8 m/s). The vertical extent is from the bottom of the mixed layer (20 m below the ocean free surface) to about 10 m above the seafloor. The isotherms in the thermocline oscillate up and down with 20–60-m peak-to-peak amplitudes (note that vertical oscillations of different isotherms are not exactly in phase as indicated by the baroclinic structure).

Within the section across the shelfbreak (Fig. 11), our simulations show the train of wave patterns moving up the slope and shelf, across the shelfbreak. Again, the diagonal panels are close to being in phase, while the most (second) off-diagonal panels are close to being in opposition of phase with these diagonal panels for the semidiurnal period. The internal tide wavelength at this location and time is found to be within 40–60 km. The largest sound-speed amplitudes of the waves in this section are around 4–5 m/s (8–10 m/s peak-to-peak amplitudes).

The internal tide variability that our simulations revealed (Figs. 10 and 11) was found to have a significant impact on our simulated broadband TL in the acoustic region. These results are illustrated now. Specifically, the variations in time of our Nx2-D TL simulations of events A and B are shown

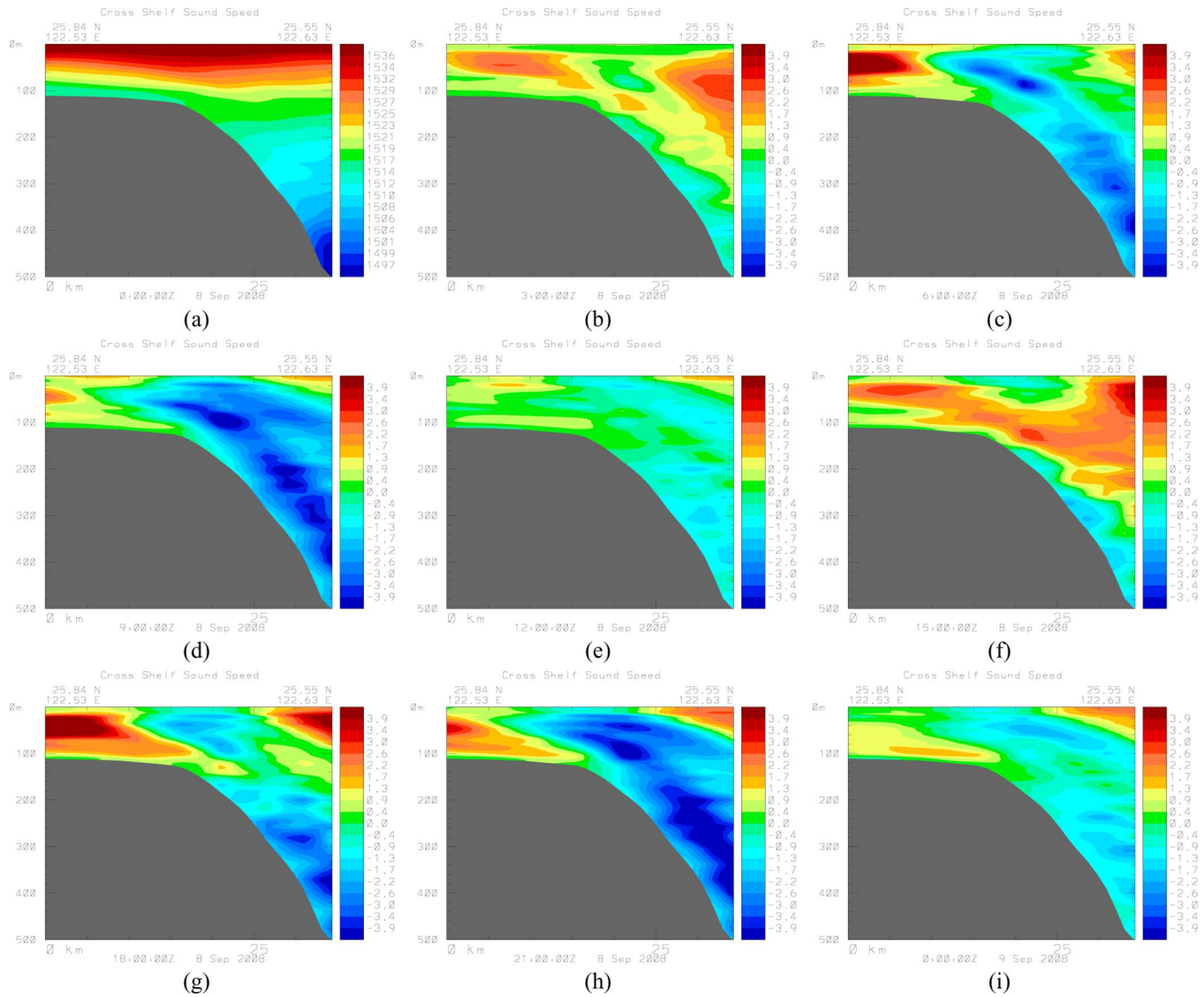

Fig. 11. Predicted sound-speed variability section from the central ocean fields, across the shelf, within the acoustic region (colorbars in meters per second): (a)–(i) times from 00:00:00Z September 8, 2008 to 00:00:00Z September 9, 2008 with 3-h intervals. (a) Total sound speed on 00:00:00Z September 8, 2008. (b)–(i) Differences between the subsequent fields and this 00:00:00Z September 8, 2008 field.

in Fig. 12 again for the day (September 8, 2008) when the two OMAS runs occurred at sea. The nine different times still refer to 3-h intervals. Fig. 12(a) is the total broadband TL on 00:00:00Z September 8, 2008 (from 65 to 105 dB, with respect to a 1-m source). Fig. 12(b)–(i) are the differences between the subsequent 3-h TLs and this 00:00:00Z September 8, 2008 TL. Note that the scale for the differences is -10 to 10 dB.

Concentrating first on the shelf (event A, blue curves), we predict relatively isotropic broadband TL variations (much more isotropic than for event B, red curves): in other words, thermocline motions due to internal tides lead to TL variations on the shelf that are more uniform with bearing angles than they are across the shelfbreak (event B). This is because the 6-km range of OMAS transmissions is smaller than half-a-wavelength of the internal tides (see Figs. 10 and 11). Hence, for the relatively flat shelf bathymetry, the oscillating depth and recurring slopes of the thermocline govern our predicted TL over 6-km range: see the similarity between the differences of the first lower diagonal [Fig. 12(d) and (h)], first upper diagonal [Fig. 12(b) and (f)], and second off-diagonal [Fig. 12(c) and (g)]. Note also that differences are close to zero on the main diagonal (panels e and i: on bearing average, -0.5 and 0.9 dB, respectively). The largest differences reach 5–10 dB at certain times. For the bearing averages, the differences are largest for panels d and h: 3.1 and 4.6 dB, respectively. TL variability and sound-speed variability are not exactly in phase, in part due to the nonlinear coupling and to the 4-D processes.

Over the shelfbreak (event B, red curves), the differences between TL curves at different times are anisotropic and rapidly variable with bearing angles. At sea, it would thus be harder to distinguish coherent internal tide effects above the shelfbreak. This is because the steep and complex bathymetry amplifies the internal tide oscillations into intricate bearing-dependent patterns: bottom bounces at slightly different locations actually occur at very different depths and slope angles, leading to very different transmissions. This leads to standard deviations that

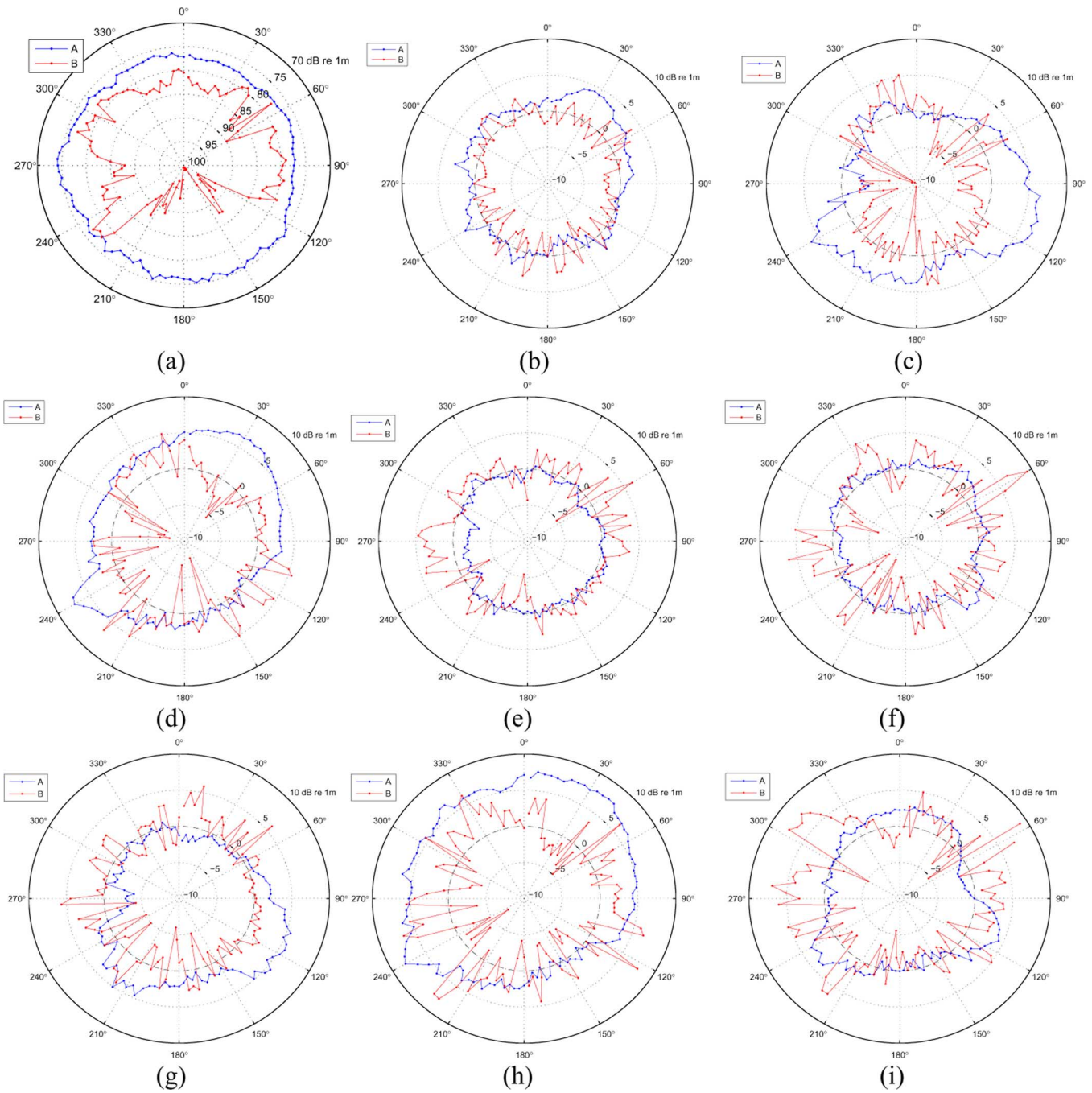

Fig. 12. Nx2-D TL simulations of event A (blue curves, $\overline{\sigma_{\mathrm{TL}_{\mathrm{tide}}}(\theta)} = 2.21$ dB) and event B (red curves, $\overline{\sigma_{\mathrm{TL}_{\mathrm{tide}}}(\theta)} = 3.29$ dB, in the bearing angle ranges: $\geq 260°$ or $\leq 110°$; $\sigma = 7.64$ dB for whole circle at different times). (a)–(i) Times from 00:00:00Z September 8, 2008 to 00:00:00Z September 9, 2008 with 3-h intervals. This includes the period during which events A and B actually occurred at sea. (a) Total TL on 00:00:00Z September 8, 2008. (b)–(i) Differences between the subsequent TL fields and this 00:00:00Z September 8, 2008 field. The TL range for these differences is from -10 to 10 dB: the dashed circle denotes 0 dB. The ocean sound speeds are those of the central ocean simulation (see parameters in the Appendixes).

are larger over the shelfbreak (event B) than over the shelf (event A), e.g., 3.29 versus 2.21 dB. However, the bearing-averaged differences are much smaller over the shelfbreak than over the shelf, as shown above. Over the shelfbreak, the largest bearing-averaged differences are only -1.4 and 1.4 dB, for Fig. 12(c) and (i), respectively, while on the shelf, they reach 4.6 dB for Fig. 12(h). Our simulation results are overall in accord with observations of [26] for the South China Sea and canonical simulations of [61], even though amplitudes are different. Finally, the TL over the shelfbreak (event B) is much higher between 120° and 260° than the TL over the shelf (event A), regardless of the internal tide properties (phase, etc.). The steep bathymetry (and not the internal tides) explains the lack of transmissions within these angles at the location and time of this shelfbreak event B.

To show detailed effects of internal tides on the TL, full vertical sections are plotted in Fig. 13. They correspond to the 0° due north section in Fig. 12. Specifically, they are: Fig. 13(a) and (b)—sound-speed sections at 12:00:00Z and 21:00:00Z on September 8, 2008;

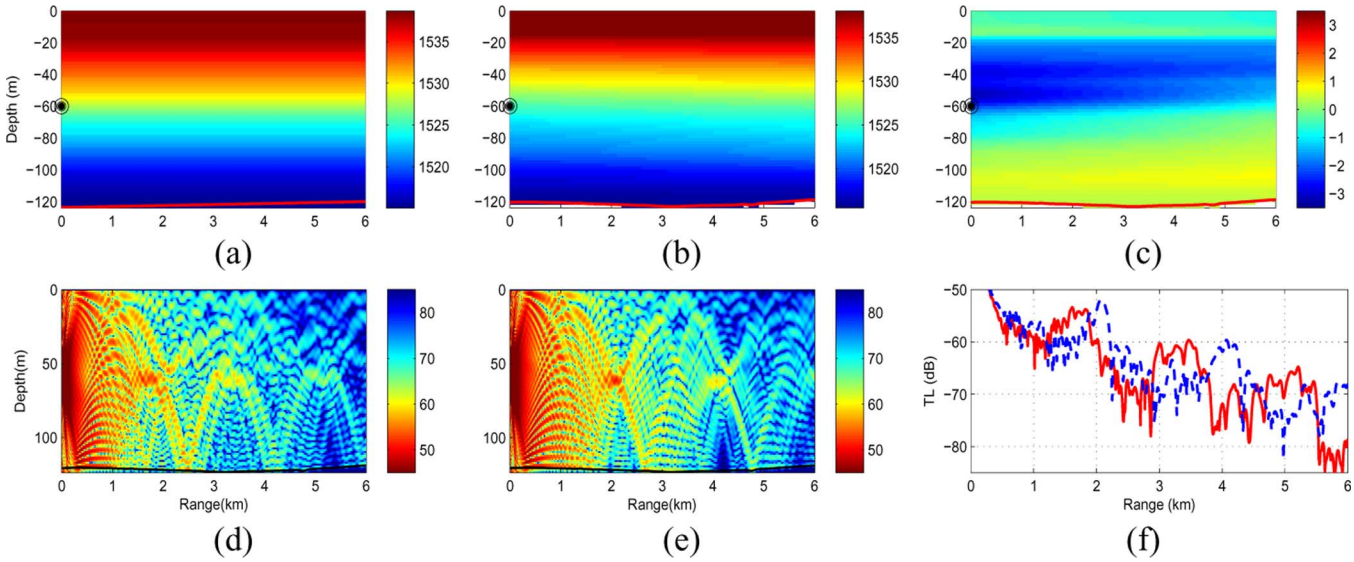

Fig. 13. Sections on September 8, 2008 in the central ocean and TL simulations [colorbar units: for (a)–(c), units are meters per second; for (d) and (e) units are decibels]: (a) sound speed at 12:00:00Z; (b) sound speed at 21:00:00Z; (c) difference of sound speeds between (a) and (b); (d) TL estimate at 12:00:00Z; (e) TL estimate at 21:00:00Z; (e) TL estimates for a receiver at 61 m, at 12:00:00Z (red) and 21:00:00Z (blue).

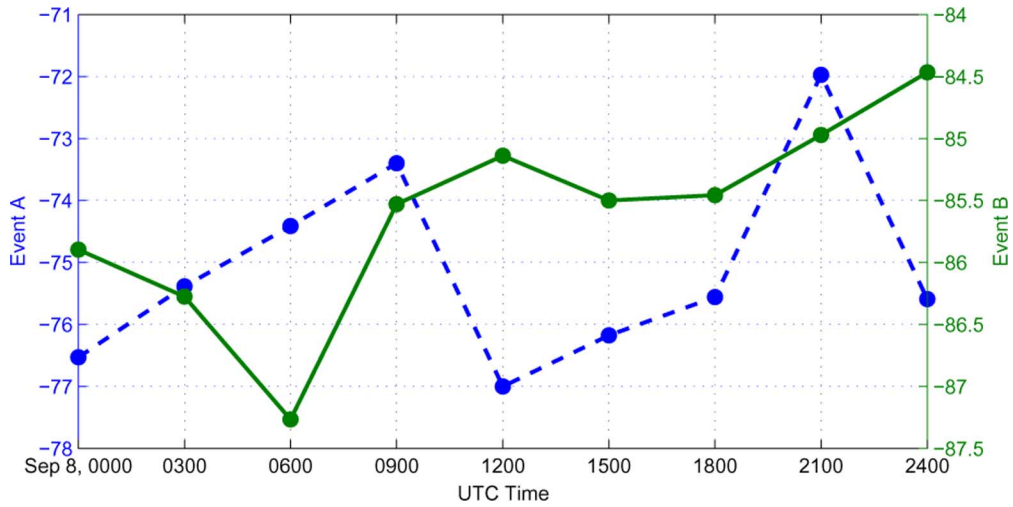

Fig. 14. Bearing-averaged TL estimates for events A and B every 3 h during September 8, 2008, computed using the central ocean sound-speed and acoustic fields.

Fig. 13(c)—difference between these two sections (9 h apart); Fig. 13(d) and (e)—full-field TL sections for these two times; and Fig. 13(f)—the same TL estimates, but at a receiver depth of 61 m. As seen from Fig. 13(a)–(c), after 9 h, the thermocline is up by more than 10 m [note that Fig. 13(c) is close to being a zoom in Fig. 11(d), around 120-m depth]. The vertical motion of the thermocline modifies the sound-speed interface structure. As seen in Fig. 13(d)–(e), this increases the width of the TL convergence zone from 1.6 to 2 km and causes more than 10-dB variation in TL at 61-m and at 6-km range, as shown in Fig. 13(f).

In Fig. 14, we show, for both events A and B, our predicted bearing-averaged TL as a function of time during September 8, 2008. Interestingly, we find that the TL around the times of event A (12:00:00Z) and, to a lesser extent, event B (15:00:00Z), are within an internal tide period corresponding to higher loss; see also Fig. 12. For event A, TL variations are due mostly to thermocline oscillations driven by internal tides and peak-to-peak amplitudes are large, reaching 8 dB. This is significant because our TL is a broadband estimate computed by range and depth averaging (see start of Section III). For the single frequency TL [continuous wave (CW), computed prior to averaging], we find that these variations have amplitudes of 20 dB. The averaging reduces the amplitudes, but they are still 5 dB. In conclusion, effects of internal tides on the shelf correspond to the largest TL sensitivity that we have found among all factors studied above, almost in par with those due to very different seabed properties (see Fig. 3).

From our computations along 120 bearings, we estimate the pdf for the uncertainty that would occur if the TL estimator available did not resolve bearing angles. These pdfs are shown in Figs. 15 and 16 for events A and B. The shape of these pdfs is time dependent during the day mostly because of semidiurnal tidal effects. For the shelf event A (Fig. 15), the TL uncertainties

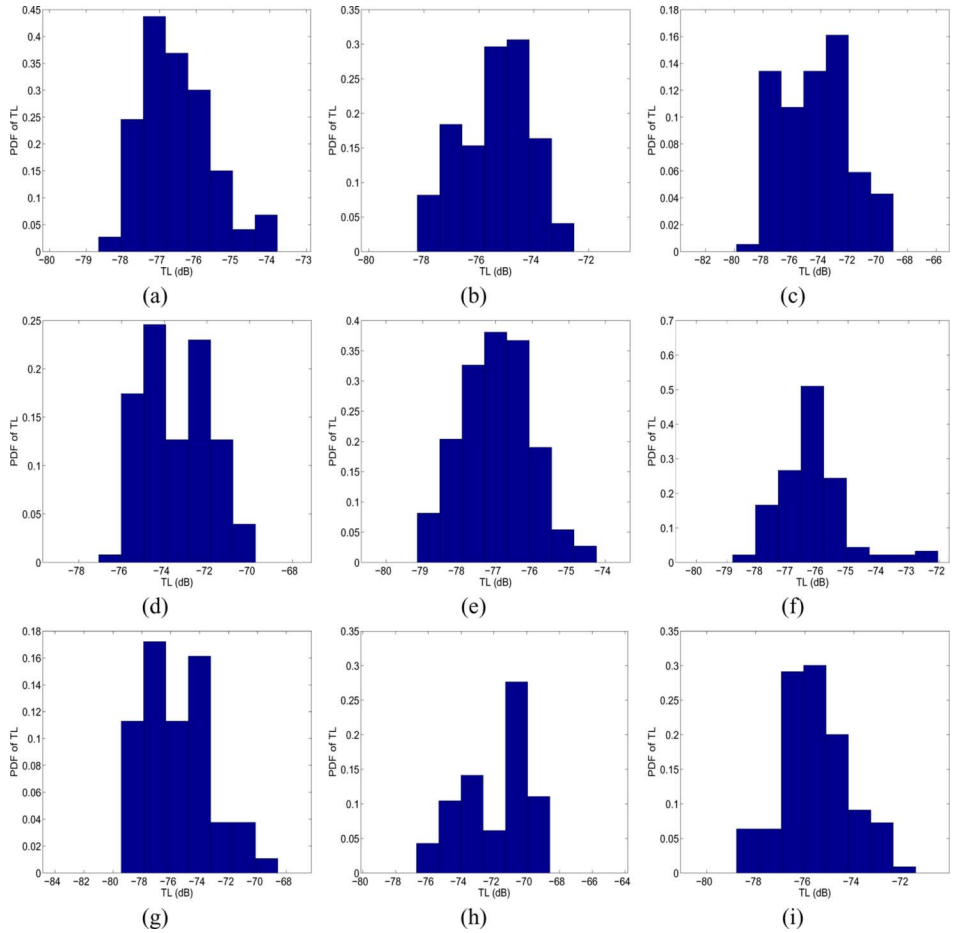

Fig. 15. PDF of TL estimates due to uncertainties in bearing angles for event A: (a)–(i) Times from 00:00:00Z September 8, 2008 to 00:00:00Z September 9, 2008 with 3-h intervals. The ocean sound speeds are those of the central ocean simulation.

in bearing are slightly skewed towards lower TL on September 8, 2008 at 00:00:00Z, 12:00:00Z, and 24:00:00Z (the diagonal of Fig. 15) but are close to being Gaussian. However, the first off-diagonals [Fig. 15(b) and (f), (d) and (h)] which are 3-h off from those on the main diagonal show TL uncertainties that are bimodal, with both high- or low-loss possible. This corresponds to the elongated TL ellipse of Fig. 12, i.e., there is a principal direction with high loss and another with low loss. Finally, the second off-diagonals [Fig. 15(c) and (g)] are again slightly skewed towards lower TL, but with twice the higher standard deviations than 6 h before or after (the panels on the diagonal). These results confirm the significance of the semidiurnal tides on the statistics of the TL on the shelf. Similar comments can be made for Fig. 16, except that in this shelfbreak case, all TL uncertainties are skewed towards high loss and bimodal (the shelf versus slope directions). The mean and standard deviations of the TL are then also much larger than on the shelf.

IV. Summary and Conclusion

This study was motivated by the striking difference in acoustic transmission data collected on the shelf and shelfbreak in the northeastern Taiwan region within the context of the QPE 2008 pilot experiment [28]. On the shelf, the mean acoustic transmission from a sound source moving for 6 h along a circular track showed little TL variation with respect to bearing angles. The largest variations there were increased loss along the northeastern direction but with small amplitudes. However, on the shelfbreak, the data for the same type of circular tracks showed no transmission when the moving source was in the deeper waters [28]. In this study, we quantified the dynamics and its uncertainties. To do so, realistic and coupled oceanographic (4-D) and acoustic (Nx2-D) field estimation with ocean data assimilation was employed and field estimates were compared to the acoustic observations available. Predictive skill, uncertainties and variability in time and space were all quantified. Specifically, using an ensemble approach, we studied the sensitivity of our results to uncertainties in a varied set of factors, including geoacoustic parameters, bottom layer thickness, bathymetry, and initial transport conditions in the region. We also quantified spatial and temporal effects of internal tide forcing on the sound-speed field and acoustic transmission field, both on the shelf and over the shelfbreak.

From our coupled simulations, we revealed that there were about 20 dB higher TLs in event B when the sound source was in the deep water region on the shelfbreak. We showed that this dramatic increase in TL is due to the deeper and complex bathymetry. This is because when the sound source moved to the steep shelfbreak region with up-slope transmission, the sound propagated down at depth trapping much energy into the bottom and resulting in a TL much higher than the TL in

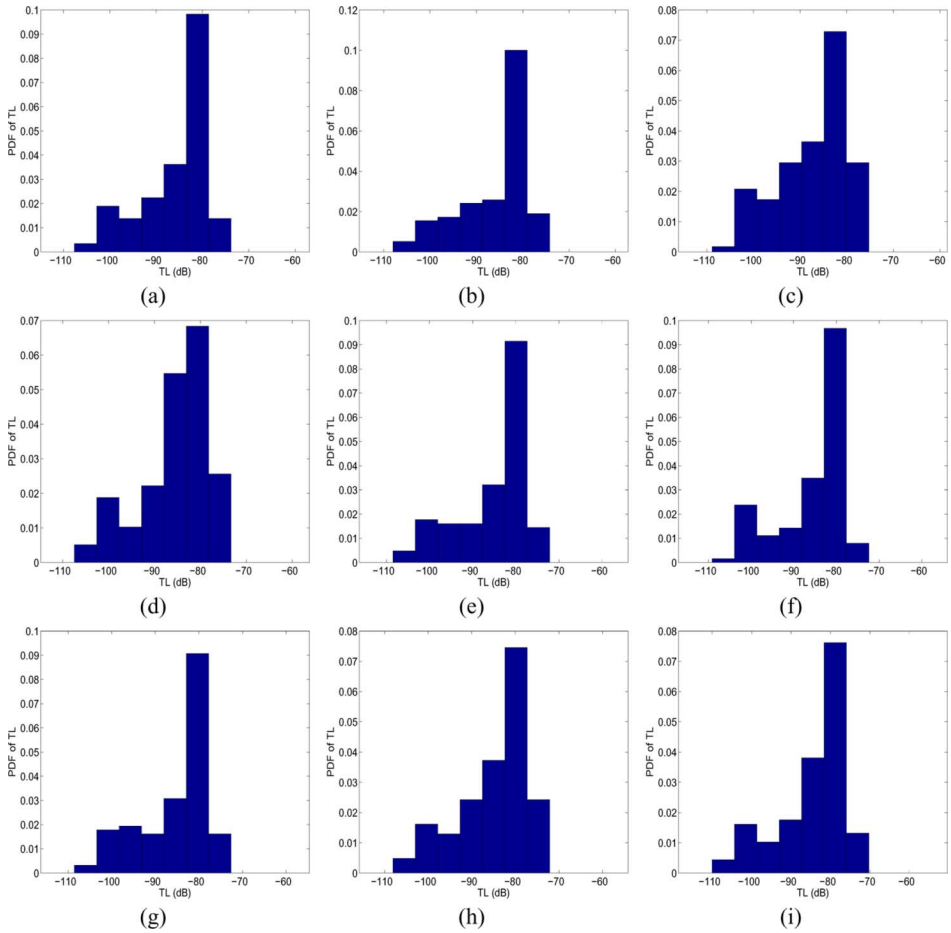

Fig. 16. PDF of TL estimates due to uncertainties in bearing angles for event B: (a)–(i) Times from 00:00:00Z September 8, 2008 to 00:00:00Z September 9, 2008 with 3-h intervals. The ocean sound speeds are those of the central ocean simulation.

the reverse direction with down-slope propagation over the shallower shelf.

In addition, we investigated uncertainties in geoacoustic parameters in both the shelf and shelfbreak acoustic simulations. We found that the sediment layer's properties led to larger but isotropic variations on the shelf (event A) and smaller but more anisotropic variations over the shelfbreak (event B). Our hybrid depth-dependent geoacoustic model for the shelfbreak and sand model for the shelf best agreed with the observations. Our investigations on the thickness of sediments showed that it had some limited effects (up to about 2 dB), but only on the up-slope transmissions on both events A and B. We also estimated the pdfs of the TL in response to these geoacoustic parameter uncertainties. We found that uncertainties in sediment sound speeds led to skewed or bimodal pdfs for the TL.

By comparing different sources and resolutions of accurate bathymetric data sets, we derived a statistical model of bathymetric uncertainties. Sensitivity studies on these uncertainties revealed that TL uncertainties (up to 1-dB standard deviation) were proportional to the 1%–4% bathymetric uncertainties but that the mean TL curves did not change their shape as a function of bearing angles.

The coupled oceanographic–acoustic modeling studies uncovered a surprising result: initial transport conditions in the Taiwan Strait can affect acoustic transmissions downstream more than 100 km away. We found that it affected the shelfbreak region (1-dB standard deviation , up to 5 dB) more than the shelf region (0.5-dB standard deviation , up to 3 dB). This is because the shelfbreak ocean dynamics is more sensitive to this transport than the shelf dynamics. The TL pdfs showed similar properties.

Using our data-assimilative ocean–acoustic modeling approach, we described and studied internal tide patterns over the shelf and slope region north of Taiwan and quantified their effects on TL in the acoustic region. The revealed wave patterns were depth dependent (baroclinic) and close to semidiurnal tidal period, affecting the whole thermocline and extending over more than 200 km on the shelf. One type of waves found were shelfbreak internal tides propagating up-slope with wavelengths around 40–80 km and horizontal phase speeds of 0.5 to about 1 m/s. Isotherms were simulated to oscillate up and down with peak-to-peak amplitudes of 20–60 m. We discovered that these variations had significant effects on the TLs over 5–6-km range: on the shelf, variations of broadband TL estimates were more isotropic and relatively larger (up to 5 dB larger) than on the shelfbreak where variations varied rapidly with bearing angles due to the steeper and more complex bathymetry. Overall, internal tides on the shelf led to the largest TL sensitivity that we simulated. For ranges of O(1–10 km), this is a signal that can be exploited. In fact, it is also seen in the intraday variability of the TL pdfs.

There are several future research activities related to our work and results. A direction is linked to the computational cost of our extensive uncertainty and sensitivity studies (see Appendix II). The use of many task and cloud computing [29] appears promising. Further work also includes modeling the effects of the drifts of the OMAS sound source and of the sonobuoy receiver during the experiment since these drifts were mostly accounted for in the processed data and in our simulations setup. For the up-slope transmissions, we also did not discuss backscattering effects that could arise due to possibly large-rock formations and volcanic effects over the shelfbreak. The azimuth angle coupling of 3-D sound propagation would also affect our TL estimates, especially further near the Canyon regions. Our coupled results helped prepare for the QPE intensive observation period in the region. In general, we expect that they will be useful for diverse applications, including determining optimum sampling plans, exploiting features, and improving 4-D coupled acoustic–ocean data assimilation and predictions.

Appendix I
Coupled Ocean–Acoustic Dynamical Models

A. Ocean Physics Model

The equations of motion are the primitive equations, derived from the Navier–Stokes equations under the hydrostatic and Boussinesq approximations [36], [62]. Under these assumptions, the state variables are the horizontal and vertical components of velocity $(\vec{u}, w)$, the temperature T, the salinity S, and the free surface elevation η. Denoting the spatial positions as (x, y, z) and the temporal coordinate with t, the primitive equations can written as

$$\text{Cons. Mass} \quad \nabla\vec{u} + \frac{\partial w}{\partial z} = 0 \tag{4}$$

$$\text{Cons. Horiz. Mom.} \quad \frac{D\vec{u}}{Dt} + f\hat{k} \times \vec{u} = -\frac{1}{\rho_0}\nabla p + \vec{F} \tag{5}$$

$$\text{Cons. Vert. Mom.} \quad \frac{\partial p}{\partial z} = -\rho g \tag{6}$$

$$\text{Surf. Elevation} \quad \frac{\partial \eta}{\partial t} + \nabla\left(\int_{-H}^{\eta} \vec{u}dz\right) = 0 \tag{7}$$

$$\text{Cons. Heat} \quad \frac{DT}{Dt} = F^T \tag{8}$$

$$\text{Cons. Salt} \quad \frac{DS}{Dt} = F^S \tag{9}$$

$$\text{Eq. of State} \quad \rho = \rho(z, T, S) \tag{10}$$

$$\text{Eq. of Sound Speed} \quad c(x, y, z, t) = C(T, S, p) \tag{11}$$

where D/Dt is the material derivative, ∇ is the horizontal gradient, f is the Coriolis parameter, p is the pressure, ρ is the density, ρ_0 is the (constant) density from a reference state, g is the acceleration due to gravity, H is the water depth in the static ocean, and $\hat{k}$ is the unit direction vector in the vertical direction. The turbulent subgridscale processes are represented by $\vec{F}$, F^T, and F^S. The vertical coordinate system is topography following.

The values of the main numerical and physical ocean parameters used in the central ocean simulations are listed in Table III1) and 2) (we refer to [36] for numerical schemes). In the horizontal direction, a Shapiro filter filters numerical noise in the state variables (F_u, F_v, F_T, F_S, F_F, and F_η in Table III). The vertical mixing is a Laplacian mixing, but with a local eddy coefficient (see [63] for details). Near the sea surface, a mixing-layer model evaluates the local "Ekman depth" $h^e(x, y, t)$, which is proportional to the coefficient E_k and the atmospheric forcing. The final h^e is constrained by adjustable bounds $h^e_{\min} \leq h^e \leq h^e_{\max}$. The vertical eddy coefficients within h^e are set to A^e_v and K^e_v. Below h^e, interior eddy coefficients are estimated based on the local gradient Richardson number Ri, the parameters being the background coefficients A^b_v and K^b_v, and shear eddy viscosity at $\mathrm{Ri} = 0$, denoted by ν_0 (Table I). For negative Ris, the convective values A^{cvct}_v and K^{cvct}_v are used. These coefficients A^{cvct}_v and K^{cvct}_v are also used at all depths and locations where the water column is statically unstable. At open boundaries, conditions similar to Perkin's [51] are employed [36]. Initially, for the central simulation, the transport through the Taiwan Strait is set to 1 Sv south and the Kuroshio transport is set based on sea-surface height and hydrographic data and geostrophic constraints [36]. Across coastlines, the normal flow and tracer flux are set to zero. Along coastlines, the tangential flow is weakened using a Rayleigh friction of relaxation time τ_c and Gaussian decay horizontal scale L_c (Table III). At the bottom, a dynamic stress balance is applied to the momentum equations, with a drag coefficient C_d. An additional Rayleigh friction of relaxation time τ_b and Gaussian decay vertical scale H_b is employed to parameterize a simple bottom boundary layer for momentum.

B. Acoustics Model

To predict the TL in the simulated ocean described above, where sound speed c is a function of (x, y, z, and t), we apply the "frozen field approximation" for the duration of sound propagation, i.e., the sound travels much faster than the ocean changes. However, for every TL computation, the ocean field and c change with time. The TL fields are computed using the normal modes code called the "coupled SACLANTCEN normal mode propagation loss model" (CSNAP, [14], [53]). It was developed as a range-dependent propagation loss model based on a widely used and efficient range-independent normal mode code SNAP [64], and a numerical solution technique for one-wave mode coupling obtained from KRAKEN. C-SNAP generalizes the range-independent problem to a range-dependent one by dividing the propagation path in a sequence of range-independent segments and using normal modes to represent the acoustic field in each segment. It uses a finite-difference algorithm to solve for the range-independent problem.

Considering first one of these segments, where c is locally assumed, only a function of z, C-SNAP uses cylindrical coordinates $(0, z_s)$ to solve the point source problem in the ocean [density and sound speed given in (10)–(11)] and seabed (density and sound speed given in Table I). The Helmholtz equation of this problem [for simplicity, denoting $\rho(z)$ and $c(z)$] for the whole ocean-seabed medium) is

$$\frac{1}{r}\frac{\partial}{\partial r}\left(r\frac{\partial p}{\partial r}\right) + \rho(z)\frac{\partial}{\partial z}\left(\frac{1}{\rho(z)}\frac{\partial p}{\partial z}\right) + \frac{\omega^2}{c^2(z)}p = -\frac{\delta(r)\delta(z - z_s)}{2\pi r} \tag{12}$$

TABLE III
COUPLED OCEAN–ACOUSTIC MODELING PARAMETERS

1) Ocean Modeling Numerical parameters	
Centroid latitude and longitude	24.501 N -122.4445 E
Domain extension	656 km(x), 728 km(y)
Grid resolution	4.0 km
Grid size	164 (x),182 (y), 70 (levels, double sigma)
Time step	100 s
State vector size	8,446,984
2) Ocean Modeling Physical parameters	
Horizontal mixing/ shapiro filter	F_u, F_v : 4-1-1; F_T , F_S : 4-1-1; F_F : 2-1-1; F_η : 2-1-1
Surface vertical mixing response to atmospheric forcing (Ekman layer)	$E_k = 0.099$; $h^e_{min} = 1$ m; $h^e_{max} = 50$ m; $A^e_v = 30\ 10^{-4}$ m^2 s^{-1} ; $K^e_v = 5\ 10^{-4}$ m^2 s^{-1}
Interior shear vertical mixing	$A^b_v = 10^{-4}$ m^2 s^{-1}; $K^b_v = 10^{-5}$ m^2 s^{-1}; $v_0 = 10^{-2}$ m^2 s^{-1} $A^{cvct}_v = 10^{-2}$ m^2 s^{-1}; $K^{cvct}_v = 10^{-2}$ m^2 s^{-1}
Open boundary conditions	$\hat{u}$, $\hat{v}$, T, S, η, $\overline{U}$, $\overline{V}$: Perkin's type boundary condition [36]
Drag coefficient	$C_d = 0.0025$
Rayleigh coastal friction	$\tau_c = 3000$ s; $L_c = 4$ km
Rayleigh bottom friction	$\tau_b = 3000$ s; $H_b = 1.5$ bottom levels
3) Coupled Ocean-Acoustic Modeling Numerical parameters	
The ocean sound speed field is linear interpolated in the horizontal, vertical, and azimuthal directions to the following resolutions:	
Horizontal direction	12.5 m
Vertical direction	2 m
Azimuthal direction	Every 3 degrees in 360 degrees circle
4) Acoustic Modeling Numerical parameters	
Minimum order mode included in the source field	$M_{min} = 1$
Maximum order mode included in the source field	$M_{max} = 1200$
Maximum order mode included in the propagating field	$M_{prop} = 1200$

where r is the range and z_s is the source depth. The normal mode representation of the acoustic pressure is given by

$$p(r,z) = \frac{i}{4\rho(z_s)} \sum_{m=1}^{\infty} \Psi_m(z_s)\Psi_m(z) H_0^{(1)}(k_m r) \qquad (13)$$

where Ψ_m is the mode amplitude, $H_0^{(1)}$ is the zero-order Hankel function of the first kind, and k_m is the eigenvalue. The solution is chosen to be limited to the outgoing traveling wave (one-way propagation), as ocean acoustic problems are often dominated by this component only.

To link the sequence of range-independent segments, and so model the range-dependent case $(c(r,z))$, C-SNAP proceeds as follows: find the normal modes, the eigenvalues, and the associated properties for each segment; compute the acoustic field on a vertical slice at the sector boundary; project this field onto the new mode set in the adjacent sector to determine modal coupling coefficients; and then repropagate the field through the next sector. This procedure is repeated for each new segment. Furthermore, to preserve accuracy, the interface condition suggested by Collins and Westwood [65] is implemented in C-SNAP. This approach, which is referred to as an impedance matching technique, consists in matching $p/(\rho c)^{1/2}$ across each interface of segments.

The values of the main numerical and physical acoustics parameters are listed in Tables III3) and III4). The resolutions used for the sound-speed segments in the horizontal, vertical, and azimuthal directions are first given. The acoustic resolution is the same in range (horizontal). Other parameters for the acoustics include the order of modes included in the source $M_{\min}$, $M_{\max}$ and propagating fields M_{prop}. We note that number of propagating modes in our study cases is of the order of 400. The physical acoustic parameters of the central simulation are the sound-speed, density, and attenuation coefficients for sand (1562 m/s, 1900 kg/m^3, 0.9 dB/λ), muddy sand (1549 m/s, 1488 kg/m^3, 1.15 dB/λ), and clay (1460 m/s, 1421 kg/m^3, 0.1 dB/λ). This is the hybrid and depth-dependent model of Table II and the optimum values of Table I.

To estimate a broadband TL, range and depth averages of CW TLs were used. Specifically, the TLs of each CW simulation were computed at all positions that were within $\pm$ 600 m in range and $\pm$5 m around the depth of the receiver. These TLs were then first averaged in depth (six samples in 10-m depth) and then triangle window (C. Emerson, personal communication) weighted averaged in range (13 samples in 1200-m range).

Appendix II
Numerical Procedures for Coupled and Realistic Modeling

The one-way coupling of ocean and acoustic computations requires specific procedures, including the interpolation of ocean fields to the acoustic grids and the matching of bathymetries for the different acoustic and ocean resolutions. It also involves the numerical coupling proper, either online during runtime or offline after the ocean model runs are completed (which is what is done here). Such procedures are summarized next. We note that they are not very different from those involved in the one-way or two-way nesting of ocean models [36], the main difference is that the one-way ocean–acoustics coupling problem here is truly multiphysics. They are also similar to one-way biological–physical coupling of PDEs [66], which is also done online or offline.

Our coupling first involves linear interpolations of the ocean sound-speed fields in the horizontal, vertical, and azimuthal directions with these numerical parameters: 100 m, 2 m, and 3°. The acoustic modeling utilizes the high 100-m resolution bathymetry while the ocean modeling uses a 4-km resolution bathymetry both latitude and longitude. However, the 4-km numerical-cell average of the 100-m bathymetry is the ocean model bathymetry. Note that the ocean model bathymetry covers a much larger region than the acoustic region. It was prepared with different sources of bathymetry which include the high 100-m resolution bathymetry, but averaged to a 4-km resolution. Because of the different bathymetric resolutions and complex ocean modeling grids, the interpolation of the sound speed from the ocean modeling domain to the acoustic modeling domain must be done carefully. To avoid generating artificial fronts, the interpolation was first carried out in the horizontal direction, and then the vertical direction. Vertical extrapolations to deeper depth (100-m acoustic resolution) were based on the averaged sound-speed profile from the closest deep-water region (4-km ocean resolution).

Our uncertainty and sensitivity studies were extensive and computationally expensive. The acoustics alone required one high-resolution CSNAP simulation along every bearing angle (3°), every 3 h for one week, for two events, for several source/receiver locations, and for several ocean simulations. Since such simulations were repeated for all cases we studied and since for each uncertainty case, not one but an ensemble of usually 120 simulations were completed, a computer cluster as well as parallel algorithms were required [29]–[31]. Such effort is, if not unprecedented, far from common. The computational cost is multiplicative in each of the parameters: the total number of 2-D acoustic simulations we have run is in the 100 000.

Acknowledgment

The authors would like to thank P. J. Haley, W. G. Leslie, and O. G. Logutov for their close collaborations. They would also like to thank P. Abbot, C. Emerson, and the Ocean Acoustical Services and Instrumentation Systems (OASIS) team for the OMAS data; G. Gawarkiewicz and colleagues for the ocean data; K. Heaney, C. Holland, and C.-F. Chen for discussions on seabed properties and uncertainties; B. Calder for his bathymetry data; and D. Marble (the U.S. Office of Naval Research) and J. Cook (Naval Research Laboratory-Monterey) and D. Geiszler [Science Applications International Corporation (SAIC)] for the COAMPS and NOGAPS atmospheric products. The authors would like to thank the whole Quantifying, Predicting, Exploiting Uncertainty (QPE) team for fruitful efforts and discussions, especially G. Gawarkiewicz, T. Duda, C.-S. Chiu, B. Cornuelle, J. F. Lynch, Y.-T. Lin, P. Niiler, L. Centurioni, C. Lee, R.-C. Lien, T. Sanford, and H. Graber, as well as the QPE team members mentioned above. They would like to thank the United States and Taiwanese research vessel crews for their work and critical data they provided. Finally, they would like to thank the QPE program managers (C. Chiu, E. Levingston, D. Marble, T. Paluszkiewicz, and B. Reeder). The authors would also like to thank the reviewers for their detailed and very useful comments.

References

[1] P. Abbot, I. Dyer, and C. Emerson, "Acoustic propagation uncertainty in the shallow east china sea," *IEEE J. Ocean. Eng.*, vol. 31, no. 2, pp. 368–383, Apr. 2006.

[2] P. Abbot and I. Dyer, "Sonar performance predictions based on environmental variability," in *Impact of Littoral Environmental Variability of Acoustic Predictions and Sonar Performance*, N. Pace and F. Jensen, Eds. Norwell, MA: Kluwer, 2002, pp. 611–618.

[3] J. F. Lynch, G. G. Gawarkiewicz, C.-S. Chiu, R. Pickart, J. H. Miller, K. B. Smith, A. R. Robinson, K. Brink, R. Beardsley, B. Sperry, and G. Potty, "Shelfbreak primer an integrated acoustic and oceanographic field study in the Mid-Atlantic Bight," in *Shallow-Water Acoustics*, R. Zhang and J. Zhou, Eds. Beijing, China: China Ocean, 1997, pp. 205–212.

[4] R. H. Headrick, J. F. Lynch, J. N. Kemp, A. E. Newhall, K. von der Heydt, J. Apel, M. Badiey, C. Chiu, S. Finette, M. Orr, B. Pasewark, A. Turgot, S. Wolf, and D. Tielbuerger, "Acoustic normal mode fluctuation statistics in the 1995 Swarm Internal Wave Scattering experiment," *J. Acoust. Soc. Amer.*, vol. 107, no. 1, pp. 201–220, 2000.

[5] P. F. J. Lermusiaux and C. S. Chiu, "Four-dimensional data assimilation for coupled physical-acoustical fields," in *Impact of Littoral Environmental Variability of Acoustic Predictions and Sonar Performance*, N. Pace and F. Jensen, Eds. Norwell, MA: Kluwer, 2002, pp. 417–424.

[6] A. R. Robinson and P. F. J. Lermusiaux, A. Tolstoy, Ed., "Prediction systems with data assimilation for coupled ocean science and ocean acoustics," in *Proc. 6th Int. Conf. Theor. Comput. Acoust.*, 2004, pp. 325–342.

[7] G. Gawarkiewicz, F. Bahr, K. Brink, R. Beardsley, M. Caruso, J. Lynch, and C.-S. Chiu, "A large-amplitude meander of the shelfbreak front in the Middle Atlantic Bight: Observations from the Shelfbreak Primer experiment," *J. Geophys. Res.*, vol. 109, 2004, doi:10.1029/2002JC001468, C03006.

[8] P. F. J. Lermusiaux, C.-S. Chiu, and A. R. Robinson, Q. L. E. Shang and T. Gao, Eds., "Modeling uncertainties in the prediction of the acoustic wavefield in a shelfbreak environment," in *Proc. 5th Int. Conf. Theor. Comput. Acoust.*, May 21–25, 2001, pp. 191–200.

[9] S. Finette, "Embedding uncertainty into ocean acoustic propagation models," *J. Acoust. Soc. Amer.*, vol. 117, no. 3, pp. 997–1000, 2005.

[10] L. C. Evans, *Partial Differential Equations*, 2nd ed. Providence, RI: AMS, 2010.

[11] K. Kunisch, G. Leugering, J. Sprekels, and F. Tröltzsch, Eds., *Control of Coupled Partial Differential Equations*, ser. International Series of Numerical Mathematics, 1st ed. Boston, MA: Birkhäuser Basel, 2007.

[12] J. Geiser, *Decomposition Methods for Differential Equations: Theory and Applications*, 1st ed. Boca Raton, FL: CRC Press, 2009.

[13] D. Wang, P. F. J. Lermusiaux, P. J. Haley, D. Eickstedt, W. G. Leslie, and H. Schmidt, "Acoustically focused adaptive sampling and on-board routing for marine rapid environmental assessment," *J. Mar. Syst.*, vol. 78, no. Suppl. 1, pp. S393–S407, 2009, DOI: 10.1016/j.jmarsys.2009.01.037.

[14] J. Xu, P. F. J. Lermusiaux, P. J. Haley, W. G. Leslie, and O. G. Logutov, "Spatial and temporal variations in acoustic propagation during the PLUSNet07 exercise in Dabob Bay," *POMA*, vol. 4, pp. 175–187, 2008, DOI: 10.1016/j.jmarsys.2009.01.029.

[15] F. A. Lam, P. J. Haley, J. Janmaat, P. F. J. Lermusiaux, W. G. Leslie, M. W. Schouten, L. A. Raa, and M. Rixen, "At-sea real-time coupled four-dimensional oceanographic and acoustic forecasts during Battlespace Preparation 2007," *J. Mar. Syst.*, vol. 78, no. Suppl. 1, pp. S306–S320, 2009.

[16] M. Rixen, J.-C. L. Gaca, J.-P. Hermand, G. Peggion, and E. Ferreira-Coelho, "Super-ensemble forecasts and resulting acoustic sensitivities in shallow waters," *J. Mar. Syst.*, vol. 78, no. Suppl. 1, pp. S290–S305, 2009.

[17] O. Carriére, J.-P. Hermand, J.-C. L. Gac, and M. Rixen, "Full-field tomography and Kalman tracking of the range-dependent sound speed field in a coastal water environment," *J. Mar. Syst.*, vol. 78, no. Suppl. 1, pp. S382–S392, 2009.

[18] N. E. Martins and S. M. Jesus, "Bayesian acoustic prediction assimilating oceanographic and acoustically inverted data," *J. Mar. Syst.*, vol. 78, no. Suppl. 1, pp. S349–S358, 2009.

[19] J. Lynch, A. Newhall, B. Sperry, G. Gawarkiewicz, P. Tyack, and C.-S. Chiu, "Spatial and temporal variations in acoustic propagation characteristics at the New England shelfbreak front," *IEEE J. Ocean. Eng.*, vol. 28, no. 1, pp. 129–150, Jan. 2001.

[20] P. F. J. Lermusiaux, C.-S. Chiu, G. Gawarkiewicz, P. Abbot, A. Robinson, R. Miller, P. Haley, W. Leslie, S. Majumdar, A. Pang, and F. Lekien, "Quantifying uncertainties in ocean predictions," *Oceanography*, vol. 19, Special Issue on Advances in Computational Oceanography, no. 1, pp. 92–105, 2006.

[21] Y.-T. Lin, A. E. Newhall, T. F. Duda, P. F. J. Lermusiaux, and P. J. Haley, "Statistical merging of data sources to estimate full water-column sound speed in the New Jersey Shallow Water 2006 Experiment," *IEEE J. Ocean. Eng.*, to be published.

[22] P. Dahl, R. Zhang, J. Miller, L. Bartek, Z. Peng, S. Ramp, J.-X. Zhou, C.-S. Chiu, J. Lynch, J. Simmen, and R. Spindel, "Overview of results from the Asian Seas International Acoustics Experiment in the East China Sea," *IEEE J. Ocean. Eng.*, vol. 29, no. 4, pp. 920–928, Oct. 2004.

[23] J. Lynch, S. Ramp, C.-S. Chiu, T. Y. Tang, Y.-J. Yang, and J. Simmen, "Research highlights from the Asian Seas international Acoustics Experiment in the South China Sea," *IEEE J. Oceanic Eng.*, vol. 29, no. 4, pp. 1067–1074, Oct. 2004.

[24] S. Ramp, C.-S. Chiu, F. Bahr, Y. Qi, P. Dahl, J. Miller, J. Lynch, R. Zhang, and J. Zhou, "The shelf-edge frontal structure in the central East China Sea and its impact on low-frequency acoustic propagation," *IEEE J. Ocean. Eng.*, vol. 29, no. 4, pp. 1011–1031, Oct. 2004.

[25] T. F. Duda, J. F. Lynch, J. Irish, R. Beardsley, S. Ramp, C.-S. Chiu, T. Y. Tang, and Y.-J. Yang, "Internal tide and nonlinear internal wave behavior at the continental slope in the northern South China Sea," *IEEE J. Ocean. Eng.*, vol. 29, no. 4, pp. 1105–1130, Oct. 2004.

[26] T. F. Duda, J. F. Lynch, A. E. Newhall, L. Wu, and C.-S. Chiu, "Fluctuation of 400-Hz sound intensity in the 2001 ASIAEX South China Sea experiment," *IEEE J. Ocean. Eng.*, vol. 29, no. 4, pp. 1264–1279, Oct. 2004.

[27] W. A. Kuperman and J. F. Lynch, "Shallow-water acoustics," *Physics Today*, vol. 57, pp. 55–61, 2004.

[28] G. Gawarkiewicz, "Quantifying, Predicting, Exploiting Uncertainty (QPE), 2008 Pilot Experiment," Woods Hole Oceanogr. Inst., Woods Hole, MA, Aug.–Sep. 22–11, 2008, p. 48.

[29] C. Evangelinos, P. F. J. Lermusiaux, J. Xu, P. J. Haley, and C. N. Hill, "Many task computing for real-time uncertainty prediction and data assimilation in the ocean," *IEEE Trans. Parallel Distrib. Syst.*, 2010, to be published.

[30] C. Evangelinos, P. F. J. Lermusiaux, J. Xu, P. J. Haley, and C. N. Hill, "Many task computing for multidisciplinary ocean sciences: Real-time uncertainty prediction and data assimilation," in *Proc. 2nd Workshop Many-Task Comput. Grids Supercomput.*, Portalnd, OR, 2009, doi.acm.org/10.1145/1646468.1646482.

[31] MSEAS Group, "The multidisciplinary simulation, estimation, and assimilation systems," Dept. Mech. Eng., Massachusetts Inst. Technol., Cambridge, MA, Rep. Ocean Sci. Eng. 6, 2010 [Online]. Available: http://mseas.mit.edu/, http://mseas.mit.edu/codes

[32] T. Y. Tang, Y. Hsueh, Y. J. Yang, and J. C. Ma, "Continental slope flow northeast of Taiwan," *J. Phys. Oceanogr.*, vol. 29, pp. 1353–1362, 1999.

[33] P. F. J. Lermusiaux, P. J. Haley, W. G. Leslie, O. Logutov, J. Xu, and E. V. Heubel, "MSEAS QPE 2008 pilot study real-time results," 2008 [Online]. Available: http://mseas.mit.edu/Sea_exercises/QPE/

[34] C.-F. Chen and J.-J. Lin, "Three dimensional effect on acoustic transmission in Taiwan's north-eastern sea," in *Proc. Int. Shallow-Water Acoust.*, Beijing, China, 1997.

[35] T. F. Duda and L. Rainville, "Diurnal and semidiurnal internal tide energy flux at a continental slope in the South China Sea," *J. Geophys. Res.*, vol. 113, 2008, doi: 10.1029/2007JC004418, 113, C03025.

[36] P. J. Haley and P. F. J. Lermusiaux, "Multiscale two-way embedding schemes for free-surface primitive-equations in the multidisciplinary simulation, estimation and assimilation system (MSEAS)," *Ocean Dyn.*, 2010, DOI: 10.1007/s10236-010-0349-4, to be published.

[37] P. J. Haley, P. F. J. Lermusiaux, W. G. Leslie, and A. R. Robinson, "Harvard Ocean Prediction System (HOPS)," 1999 [Online]. Available: http://mseas.mit.edu/HOPS

[38] P. J. Haley, P. F. J. Lermusiaux, A. R. Robinson, W. G. Leslie, O. Logutov, G. Cossarini, X. S. Liang, P. Moreno, J. D. Doyle, J. Bellingham, F. Chavez, and S. Johnston, "Forecasting and reanalysis in the Monterey Bay/California Current region for the Autonomous Ocean Sampling Network-II experiment," *Deep Sea Res. II*, vol. 56, no. 3–5, pp. 127–148, 2009, doi:10.1016/j.dsr2.2008.08.010.

[39] A. Agarwal and P. F. J. Lermusiaux, "Statistical field estimation for complex coastal regions and archipelagos," *Ocean Model.*, 2010, submitted for publication.

[40] P. F. J. Lermusiaux, "Estimation and study of mesoscale variability in the Strait of Sicily," *Dyn. Atmos. Oceans*, vol. 29, pp. 255–303, 1999.

[41] P. F. J. Lermusiaux, A. R. Robinson, P. J. Haley, and W. G. Leslie, "Filtering and smoothing via error subspace statistical estimation," in *Advanced Interdisciplinary Data Assimilation*. New York: Holland Publications, 2002, pp. 795–802.

[42] P. F. J. Lermusiaux, "Uncertainty estimation and prediction for interdisciplinary ocean dynamics," *J. Comput. Phys.*, vol. 217, Special Issue of on Uncertainty Quantification, no. 1, pp. 176–199, 2006.

[43] P. F. J. Lermusiaux, "Adaptive sampling, adaptive data assimilation and adaptive modeling," *Physica D*, vol. 230, Special Issue on Mathematical Issues and Challenges in Data Assimilation for Geophysical Systems: Interdisciplinary Perspectives, pp. 172–196, 2007.

[44] T. P. Sapsis and P. F. J. Lermusiaux, "Dynamically orthogonal field equations for continuous stochastic dynamical systems," *Physica D*, vol. 238, pp. 2347–2360, 2009, DOI: 10.1016/j.physd.2009.09.017.

[45] R. C. Tian, P. F. J. Lermusiaux, J. J. McCarthy, and A. R. Robinson, "A generalized prognostic model of marine biogeochemical-ecosystem dynamics: Structure, parameterization and adaptive modeling," Harvard Rep. Physical/Interdisciplinary Ocean Sci., Cambridge, MA, Tech. Rep. No.67, 2008.

[46] O. G. Logutov and P. F. J. Lermusiaux, "Inverse barotropic tidal estimation for regional ocean applications," *Ocean Model.*, vol. 25, pp. 17–34, 2008, DOI: 10.1016/j.ocemod.2008.06.004.

[47] P. F. J. Lermusiaux, P. J. Haley, W. G. Leslie, O. Logutov, J. Xu, and A. Agarwal, "MSEAS real-time results for the intensive observation period," Taiwan-Kuroshio Region, 2009 [Online]. Available: http://mseas.mit.edu/Sea exercises/QPE_IOP09/

[48] M. S. Lozier, W. B. Owens, and R. G. Curry, "The climatology of the North Atlantic," *Progr. Oceanogr.*, vol. 36, pp. 1–44, 1995.
[49] B. Calder, "High resolution bathymetry," 2009 [Online]. Available: http://ccom.unh.edu/people/index.php?q=calder
[50] P. F. J. Lermusiaux, "Error subspace data assimilation methods for ocean field estimation: Theory, validation and applications," Ph.D. dissertation, Div. Eng. Appl. Sci., Harvard Univ., Cambridge, MA, 1997.
[51] A. L. Perkins, L. F. Smedstad, D. W. Blake, G. W. Heburn, and A. J. Wallcraft, "A new nested boundary condition for a primitive equation ocean model," *J. Geophys. Res.*, vol. 102, no. C2, pp. 3483–3500, 1997.
[52] P. F. J. Lermusiaux, P. J. Haley, W. G. Leslie, O. Logutov, J. Xu, and E. V. Heubel, "OR1 forecast skill metrics," 2008 [Online]. Available: http://mseas.mit.edu/Sea_exercises/QPE/Maps/Sep10/Skill/
[53] C. M. Ferla, M. B. Porter, and F. B. Jensen, "C-SNAP: Coupled SACLANTCEN normal mode propagation loss model," La Spezia, Italy, SACLANTCEN document SM-274, 1993.
[54] P. Abbot and C. Emerson, Ocean Acoustical Services and Instrumentation Systems (OASIS), 2009 [Online]. Available: http://www.oasislex.com/capabilities.htm
[55] C. H. Harrison and J. A. Harrison, "A simple relationship between frequency and range averages for broadband sonar," *J. Acoust. Soc. Amer.*, vol. 97, no. 2, pp. 1314–1317, 1995.
[56] L. M. Brekhovskikh and Y. P. Lysanov, *Fundamentals of Ocean Acoustics*, ser. Modern Acoustics and Signal Processing. College Park, MD: AIP, 2002.
[57] E. L. Hamilton, "Geoacoustic modeling of the sea floor," *J. Acoust. Soc. Amer.*, vol. 68, no. 5, pp. 1313–1340, 1980.
[58] F. B. Jensen, W. A. Kuperman, M. B. Porter, and H. Schmidt, Eds. , *Computational Ocean Acoustics*, ser. Modern Acoustics and Signal Processing. College Park, MD: AIP, 2000, pp. 36–38.
[59] K. Heaney, "Sensitivity analysis for QPE pilot study—Draft 1," OASIS, Inc., Lexington, MA, 2008, 32pp.
[60] S. Jan and S.-Y. Chao, "Seasonal variation of volume transport in the major inflow region of the Taiwan Strait: The Penghu Channel," *Deep-Sea Res. II*, vol. 50, pp. 1117–1126, 2003.
[61] S. Finette, R. Oba, C. Shen, and T. Evans, "Acoustic propagation under tidally driven, stratified flow," *J. Acoust. Soc. Amer.*, vol. 121, no. 5, pp. 2575–2590, 2007.
[62] B. Cushman-Roisin and J.-M. Beckers, *Introduction to Geophysical Fluid Dynamics: Physical and Numerical Aspects*. New York: Academic, 2010.
[63] P. F. J. Lermusiaux, "Evolving the subspace of the three-dimensional multiscale ocean variability: Massachusetts Bay," *J. Mar. Syst.*, vol. 29, Special Issue on "Three-Dimensional Ocean Circulation: Lagrangian Measurements and Diagnostic Analyses", no. 1–4, pp. 385–422, 2001.
[64] F. B. Jensen and C. M. Ferla, *SNAP: The SACLANTCEN Normal Mode Acoustic Propagation Model*. La Spezia, Italy: NATO SACLANT Undersea Res. Ctr., 1979.
[65] M. D. Collins and E. K. Westwood, "A higher order energy conserving parabolic equation for range-dependent oceandepth," *J. Acoust. Soc. Amer.*, vol. 89, pp. 1068–1075, 1991.
[66] S. T. Besiktepe, P. F. J. Lermusiaux, and A. R. Robinson, "Coupled physical and biochemical data driven simulations of Massachusetts Bay in late summer: Real-time and post-cruise data assimilation," *J. Mar. Syst.*, vol. 40, pp. 171–212, 2003.

Pierre F. J. Lermusiaux received B.S. and M.S. degrees in mechanical engineering (highest honors and Jurybs congratulations) from Liege University, Liege, Belgium, in 1992 and the S.M. and Ph.D. degrees in engineering sciences from Harvard University, Cambridge, MA, in 1993 and 1997, respectively.

Currently, he is an Associate Professor of Mechanical Engineering, Massachusetts Institute of Technology, Cambridge. His current research interests include physical and interdisciplinary ocean dynamics, from submesoscales to interannual scales. They involve physical–biogeochemical–acoustical ocean modeling, optimal estimation and data assimilation, uncertainty and error modeling, and the optimization of observing systems.

Dr. Lermusiaux has held Fulbright Foundation Fellowships, was awarded the Wallace Prize at Harvard in 1993, presented the Ogilvie Young Investigator Lecture in Ocean Engineering at MIT in 1998 and was awarded a Doherty Associate Professorship in Ocean Utilization by MIT in 2009. He is a member of the Association of Engineers of Liege University, Friends of the University of Liege, the Royal Meteorological Society, the American Geophysical Union, the Oceanography Society, the American Association for the Advancement of Science, and the Society for Industrial and Applied Mathematics.

Jinshan Xu received the B.A. degree in electrical engineering and the Sc.M. degree in physical oceanography from the University of Qingdao, Qingdao, China, in 1994 and 1999, respectively, and the Ph.D. degrees in mechanical and oceanographic engineering from Massachusetts Institute of Technology/Woods Hole Oceanographic Institute Joint Program in Oceanography, Cambridge, in September 2007.

Currently, he is a Postdoctoral Research Associate at the Mechanical Engineering Department, Massachusetts Institute of Technology, Cambridge. His research interests are in the areas of underwater acoustic propagation modeling and signal processing and wave propagation through random media.

Dr. Xu is a member of the Acoustical Society of America.

Chi-Fang Chen received the B.S. degree in naval architecture from National Taiwan University, Taipei, Taiwan, in 1981 and the M.S. and Ph.D. degrees in ocean engineering from the Massachusetts Institute of Technology, Cambridge, in 1983 and 1990, respectively.

Currently, she is a Professor at the Department of Engineering Science and Ocean Engineering, National Taiwan University. Her research interests include underwater acoustics, particularly 3-D acoustic propagation, and acoustic detection and communication.

Sen Jan received the B.S. degree in mechanical engineering from Chung Yung University, Zhongli, Taiwan, in 1986 and the M.S. and Ph.D. degrees in physical oceanography from the National Taiwan University, Taipei, Taiwan, in 1988 and 1995, respectively.

Currently, he is an Associate Professor at the Institute of Oceanography, National Taiwan University. His research interests are physical and physical–biogeochemical–coupled processes in the ocean, from coastal to regional scales.

Dr. Jan is a Member of the American Geophysical Union.

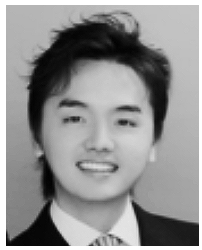

Linus Y. Chiu received the B.S. degree in hydraulic and ocean engineering from National Cheng Kung University, Tainan, Taiwan, in 2002 and the Ph.D. degree in ocean engineering from the National Taiwan University, Taipei, Taiwan, in 2008.

Currently, he is a Postdoctoral Fellow at the Department of Engineering Science and Ocean Engineering, National Taiwan University. His research interests include shallow-water acoustics, particularly acoustic propagation and underwater communication.

Yiing-Jang Yang was born in Taiwan in 1967. He received the B.S. degree in oceanography from the National Taiwan Ocean University, Keelung, Taiwan, in 1990 and the Ph.D. degree in physical oceanography from the National Taiwan University, Taipei, Taiwan, in 1996.

Currently, he is an Associate Professor at the Department of Marine Science, Naval Academy, Kaohsiung, Taiwan. His research interests include internal tides and waves and current variation around Taiwan.

Dr. Yang is a Member of the American Geophysical Union.